

A COMPARISON OF SYNOPTIC AND SKYLAB  
S193/194 DETERMINATIONS OF OCEAN  
SURFACE WINDSPEEDS

E7.6-10312

NASA CR-

147540

by

Duncan Ross

A series of low-level aircraft flights were conducted during SL2 and SL4 to provide reference information to evaluate the accuracy of SKYLAB measurements of  $\sigma_0$  and  $T_B$  and to develop and test empirically based algorithms for the determination of surface windspeed from measurements of the above parameters. The active portion of S193 was found to be usefully sensitive to variations in windspeed by both polarizations at incidence angles of about  $30^\circ$ ,  $40^\circ$ , and  $50^\circ$  for both launch periods, despite diminished performance of the antenna during SL4. During SL2, the experiment program yielded aircraft and satellite measurement of ocean surface roughness which varied from essentially calm to hurricane force (c.f. Ross, et al., 1974; Au, et al., 1974; Ross, 1975; attached as Appendix A, B, and C, respectively) which are suitable to study the relationship between microwave parameters and surface roughness.

"Made available under NASA sponsorship  
in the interest of early and wide dissemination of Earth Resources Survey  
Program information and without liability  
for any use made thereof."

(E76-10312) A COMPARISON OF SYNOPTIC AND  
SKYLAB S193/194 DETERMINATIONS OF OCEAN  
SURFACE WINDSPEEDS (National Oceanic and  
Atmospheric Administration) 76 p HC \$5.00  
CSSL 04B G3/48

N76-22861

Unclas  
00312

Given that both the active and passive portions of the microwave instruments aboard SKYLAB are sensitive to surface windspeed, the intent of this investigation was to verify this sensitivity and establish and test algorithms to determine the accuracy and precision of satellite inferred surface windspeeds.

Satellite underflights by NOAA and NASA aircraft on 5, 6, and 11 June 1973 yielded a wide range of measurements under a variety of conditions. The data of 11 June (Ross, 1975) showed that the presence of rain during low wind conditions can increase the backscattered return apparently due to generation of Bragg waves by impacting raindrops. The SKYLAB data of 6 June was obtained in conjunction with near simultaneous aircraft penetration of Pacific Hurricane AVA and yielded active and passive measurements of surface roughness from windspeeds of 10-25 m/s.

A number of studies have shown that a power law fit of the form

$$y = a_0 x^{a_1}$$

reasonably well describes the behavior of the normalized radar backscattering cross section over a wide range of wind conditions while the behavior of the naturally emitted microwave energy is approximately linear and can be modeled with a fit of the form

$$y = a_0 + a_1x$$

The data sets from 5, 6, and 11 June ( $\sigma_0$  measurements were adjusted to upwind after the technique suggested by Pierson, Cardone and Greenwood (1974) were accordingly fit by appropriate power law or least squares linear relationships with windspeed as the dependent variable for the sake of simplicity of the windspeed algorithm. The results are contained in Table I. It can be seen from the table by examination of the coefficient of determination,  $r^2$ , that the data for an incidence angle of  $44^\circ$  fit poorly ( $r^2$  would equal 1 for a perfect fit) and therefore are widely scattered. This may possibly be due to rainfall which was present in the lower wind areas of the hurricane.

The data for the incidence angle of  $51^{\circ}$ , however, yielded a maximum value for  $r^2$  of .78 which is high enough to suggest that this algorithm could be reliably used to estimate surface winds. Testing of these algorithms, however, was not carried out due to lack of extensive high quality surface truth accompanied by high winds during SL3, and damage to the antenna during SL4 which modified its characteristics thereby invalidating the algorithm.

The antenna damage during SL4 consisted of a crack in the antenna feed in the vicinity of the reflector which greatly modified the antenna pattern. Received power was therefore reduced and the purity of polarization was compromised. Extensive interesting data was obtained, however, for moderate to high winds in winter storms which were accompanied by low altitude aircraft flights. On 9 January, a particularly interesting data set was obtained in a N. Atlantic storm (Figs. 1 and 2) which was characterized by surface winds which varied from 7.5 to 30 m/s along the subsatellite track. Power law and linear least squares fits to the data yielded the coefficients shown in Table II.

Because of the questions regarding polarization purity of the transmitted radar energy and the preponderance of data for the higher winds, both linear least squares and power law fits to the  $\sigma_0$  data were carried out and gave comparably high values of  $r^2$  (.7-.8). Also, since both the scattering and reference windspeed measurement are subject to errors, a variety of algorithms by means of power law and least squares fits were obtained, some with a procedure which weighted the dependent and independent variable depending upon a specified error for each. The results are contained in Table II.

The algorithms of Table II were then utilized to estimate surface winds from SKYLAB parameters obtained on 4 January in an Atlantic storm (Fig. 3), and on 24 January in a Pacific storm (Fig. 4). The computed winds were then compared to winds determined by subjective analysis of the weather charts based mainly upon ship reports and aircraft measurements. Mean and RMS differences between the two winds are contained in Table III. Use of the algorithms for  $\sigma_0$  based upon a linear least squares fit produce comparable though slightly higher results.

As can be seen from Table III, the RMS differences between analyzed and inferred winds in the case of the passive side of S193 are higher than those resulting from the scatterometer mode. An analysis of the antenna pattern conducted by the University of Kansas indicates the effective beam width to be essentially horizon to horizon with unknown side lobe effects. Fortunately, the scale of the weather systems for the 4, 24, and 9 January situations appears to have been large enough so that surface roughness conditions could be considered homogeneous within the footprint. NIMBUS-G brightness temperature distributions at 19.5 GHz for 9 January are shown in Figure 5 and indicate similar qualitative behavior in the areas viewed by SKYLAB lending some confidence in the S193 SL4 passive results.

In order to establish a basis for assessing the quality of these SKYLAB results, the reference surface windspeeds used for the 4, 9, and 24 January data sets were compared with those produced by Dr. Vincent Cardone of CUNY who used an objective procedure based upon pressure fields but weighted in favor of ship or aircraft reports. This comparison yielded

mean and RMS differences as shown in Table IV, with the objective procedure yielding somewhat lower mean winds. It can be seen that the active portion of S193 during SL4 produces results comparable to that of either an objective or subjective analysis procedure based upon conventional data sources while the passive results are somewhat higher.

The S194 instrument operating at L-Band is also sensitive to surface roughness, though less so than the higher frequencies. The data of 9 January were therefore suitable for least squares fitting and produced the following results for vertical incidence.

$$U = -484 + 5.4 T_B$$

As with S193, the data of 4 and 24 January were used to estimate surface winds and compared to the analyzed wind field. Mean and RMS differences resulting were 4.5 m/s and 5.6 m/s, respectively.

Aircraft measurements of microwave brightness temperature at Ku band presented in Appendix A for data collected on 5 and 11 June agree with satellite measurements to about 1°.

Sensitivity of the instrument cannot be determined absolutely, but can be inferred from the low RMS errors of the estimation of surface windspeed to be better than .5 db in the case of the active portion of S193. Because of the antenna damage, comparable estimates of the performance of the passive side of S193 cannot be made. In the case of S194, the accuracy and sensitivity of the instrument appears to have been approximately 1°K.

REFERENCES

Au, B., J. Kenney, L. U. Martin, and D. Ross (1974), Multi-frequency radiometric measurements of foam and a monomolecular slick. Ninth International Symposium on Remote Sensing of Environment Proceedings, 15-19 April, 1763-1773.

Pierson, Willard J., Vincent J. Cardone, J. Arthur Greenwood (1974), The applications of SEASAT-A to meteorology. Prepared by the University Institute of Oceanography of the City University of New York for the SPOC Group of the National Environmental Satellite Service, National Oceanic and Atmospheric Administration under Grant No. 04-4-158-11, August 1974, 84 pp.

Ross, D., B. Au, W. Brown, and J. McFadden (1974), A remote sensing study of Pacific Hurricane Ava. Ninth International Symposium on Remote Sensing of Environment Proceedings, 15-19 April, 163-180.

Ross, Duncan, (1975), A comparison of SKYLAB S-193 and aircraft views of surface roughness and a look toward SEASAT. First Comprehensive Symposium on the Practical Application of Earth Resources Survey Data Proceedings, June 1975, 1911-1936.

ACKNOWLEDGEMENTS

The author regrets that the large number of plots and calculations produced during the course of this investigation must be summarized in such a brief fashion as represented in this report. Recognition must be extended, however, to Messrs. Bruce Gritton, Pete Connors, and Jim Cordova for their many hours devoted to this project, to Mr. Monte Poindexter for the excellent and tedious meteorological analyses, and to Dr. Robert Long for his advice and consultations. Special thanks are due the Flight Crews of the NOAA, NASA, and USAF aircraft for their dedication and interest in providing proper surface reference information.

TABLE I

SL 2

Parameter	Polarization	$a_0$	$a_1$	$r^2$	Incidence Angle
$\sigma_0$	VV	29.3	.33	.22	44°
$\sigma_0$	HH	58.9	.43	.37	44°
$\sigma_0$	VV	63.2	.53	.75	51°
$\sigma_0$	HH	122	.54	.74	51°
$T_B$	VV	- 65.2	.47	.68	44°
$T_B$	HH	- 45.2	.49	.75	44°
$T_B$	VV	- 12.7	.14	.45	51°
$T_B$	HH	- 38.7	.44	.78	51°

TABLE II

9 January

Parameter	Polarization	$a_0$	$a_1$	$r^2$	Incidence Angle
$\sigma_0$	VV	16.37	.55	.87	30°
$\sigma_0$	HH	24.16	.59	.78	30°
$T_B$	VV	-256.87	2.23	.59	30°
$T_B$	HH	-176.85	1.86	.84	30°
$\sigma_0$	VV	22.26	.57	.94	40.8
$\sigma_0$	HH	34.09	.59	.83	40.8
$T_B$	VV	-431.39	3.58	.91	40.8
$T_B$	HH	-238.9	2.54	.95	40.8
$\sigma_0$	VV	26.61	.61	.91	47.6
$\sigma_0$	HH	40.07	.53	.65	47.6
$T_B$	VV	-553.8	4.49	.92	47.6
$T_B$	HH	-246.9	2.8	.95	47.6

TABLE III

$\theta$	Parameter	Polarization	4 Jan		24 Jan		Incidence Angle
			Mean Diff (m/s)	RMS Diff (m/s)	Mean Diff (m/s)	RMS Diff (m/s)	
30°	$\sigma_0$	VV	2.55	2.63	2.67	2.5	32°
30°	$\sigma_0$	HH	3.53	4.10	-.85	2.54	32°
40.8°	$\sigma_0$	VV	.68	2.57	0.00	1.59	41°
40.8°	$\sigma_0$	HH	2.57	3.63	1.47	1.86	41°
47°	$\sigma_0$	VV	1.91	3.70	-1.01	2.49	48°
47°	$\sigma_0$	HH	-.9	3.73	-3.11	2.67	48°
30°	$T_B$	VV	-3.02	6.56	-4.6	5.4	32°
	$T_B$	HH	2.72	6.13	3.0	4.0	32°
40.7°	$T_B$	VV	1.99	5.04	-.8	3.4	41°
	$T_B$	HH	.69	4.35	-.4	3.5	41°
47°	$T_B$	VV	-1.71	5.27	-1.5	4.5	48°
	$T_B$	HH	-4.06	4.25	-3.3	4.7	48°

TABLE IV

Cardone vs Ross	Mean Diff (m/s)	RMS Diff (m/s)	Incidence Angle
9 Jan	-4.65	3.63	30°
	-4.10	3.21	40.7
	-2.99	3.02	47.6
4 Jan	-3.33	3.0	30
	-1.78	3.87	40
	-2.74	2.21	47
24 Jan	.02	.16	30
	-3.05	1.56	40
	-2.85	.93	50

ORIGINAL PAGE IS OF POOR QUALITY

## FIGURE CAPTIONS

Figure 1. Surface analysis for the SKYLAB underflight of 9 January 1974. Data locations at incidence angles of  $0^{\circ}$ ,  $40.7^{\circ}$ ,  $47.6^{\circ}$ ,  $42.9^{\circ}$ , and  $50.5^{\circ}$  are shown. Surface winds from ship reports are shown with the solid flags indicating 50 knot winds.

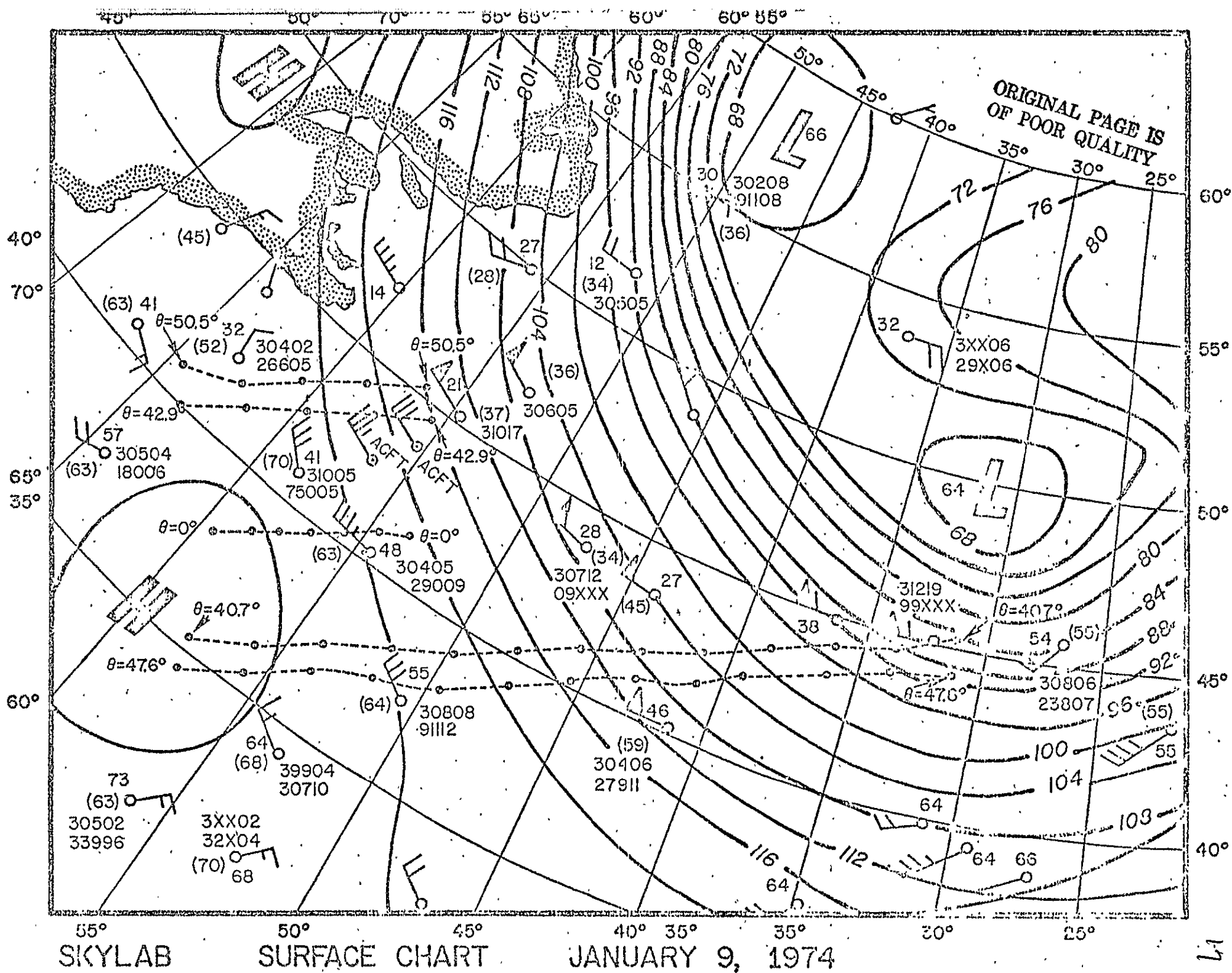
Figure 2. Brightness temperature and  $\sigma_0$  measurements adjusted to upwind are shown as a function of time for the indicated incidence angles for the 9 January S193/194 data sets. Surface winds were determined from the analysis of Figure 2 based upon ship reports.

Figure 3. Surface analysis for the 4 January data set. SKYLAB S193 data points at  $\theta=0^{\circ}$ ,  $40^{\circ}$ , and  $47^{\circ}$ , are shown.

Figure 4. Surface analysis for the 24 January data set. S193 observation points are shown along with the associated incidence angle.

## FIGURE CAPTIONS (continued)

Figure 5. Contour map of the NIMBUS-G 19.35 GHz brightness temperatures. Corresponding SKYLAB data points are superimposed on the map for incidence angles of  $50.5^{\circ}$  (A),  $42.9^{\circ}$  (B),  $0.0^{\circ}$  (C),  $40.7^{\circ}$  (D), and  $47.6^{\circ}$  (E).



# SATELLITE OBSERVATIONS 9 JANUARY 1974

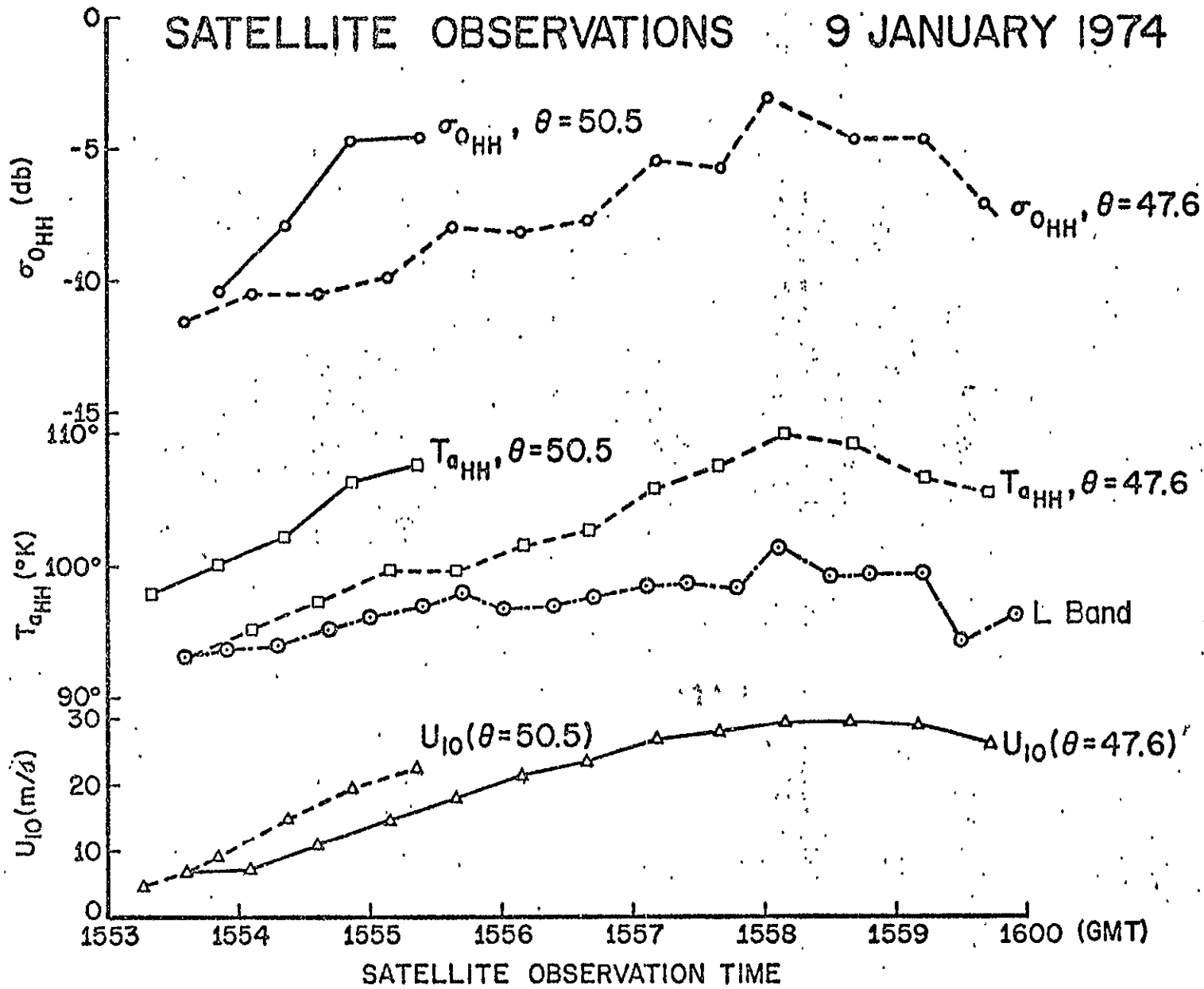
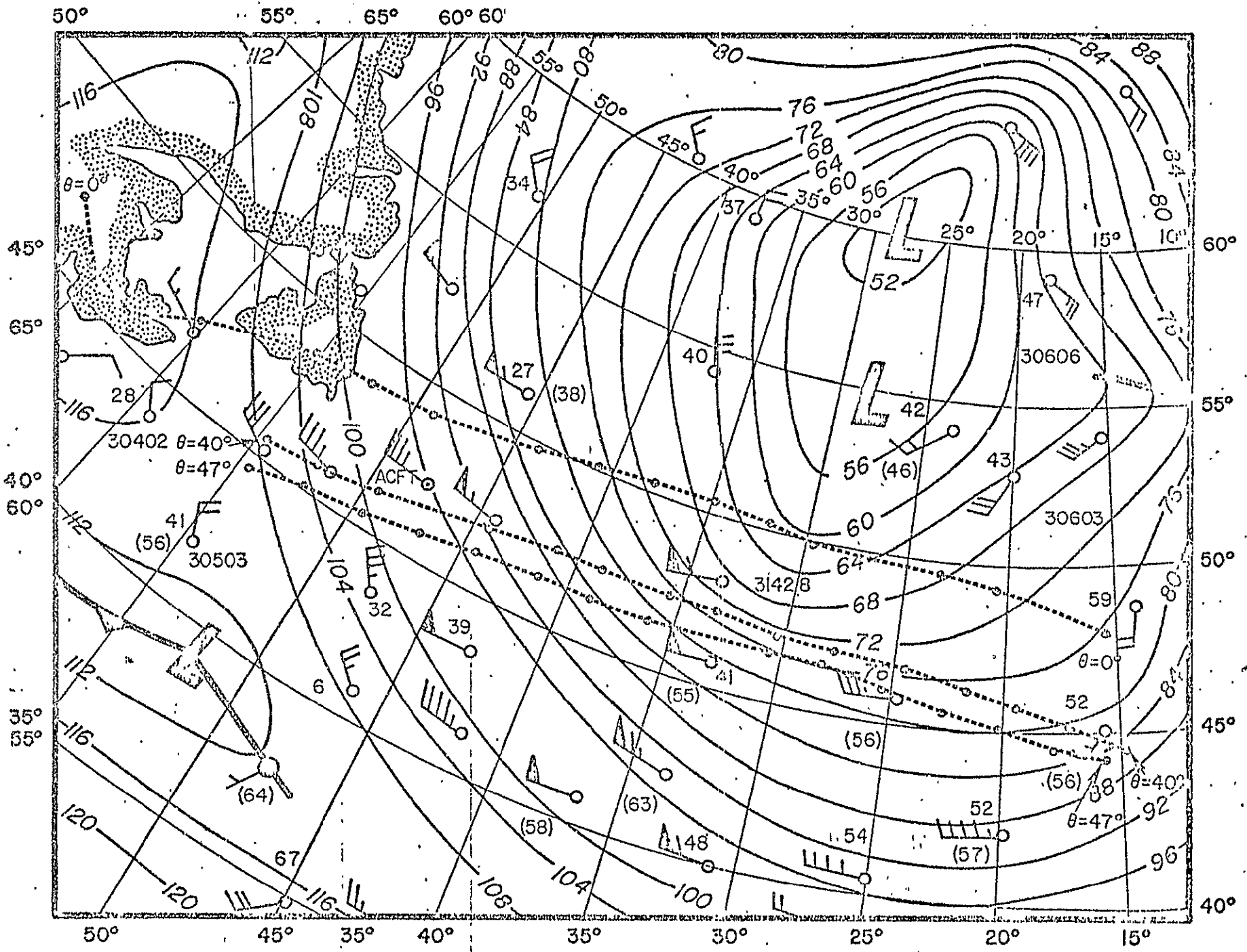


Figure 2



ORIGINAL PAGE IS  
OF POOR QUALITY

SKYLAB

SURFACE CHART

JANUARY 4, 1974

Figure 3



# NIMBUS "E" BRIGHTNESS TEMPERATURE DISTRIBUTION

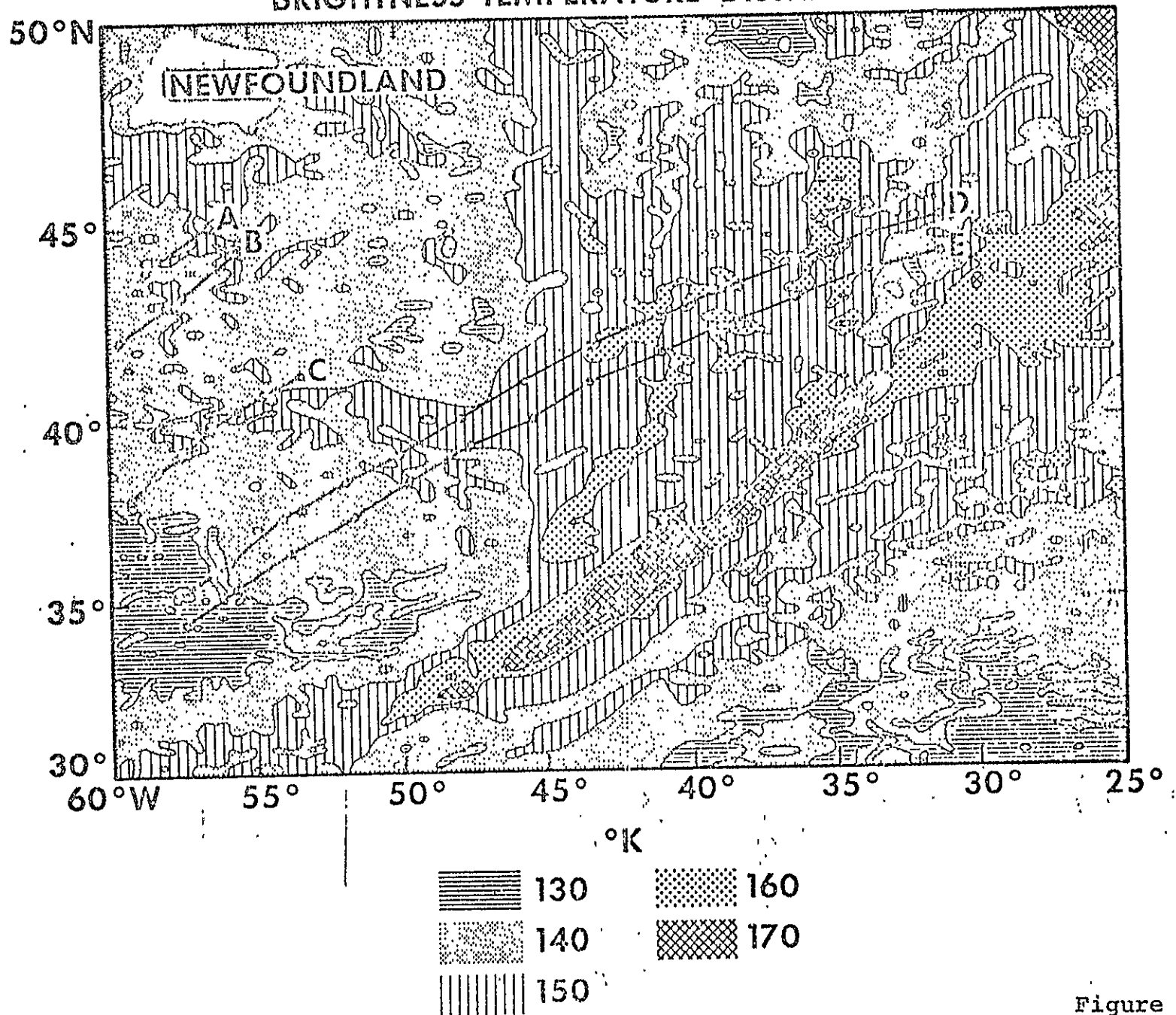


Figure 5

Appendix A

MULTI-FREQUENCY RADIOMETRIC MEASUREMENTS OF FOAM  
AND A MONO-MOLECULAR SLICK

ORIGINAL PAGE IS  
OF POOR QUALITY

B. Au, J. Kenney, L. U. Martin

Naval Research Laboratory  
Washington, D.C.

and

D. Ross

National Oceanic and Atmospheric Administration  
Miami, Florida

ABSTRACT

Microwave radiometric measurements have been made of both a surf-zone and of an ocean region where small-scale roughness was suppressed by an artificial mono-molecular slick. The foam measurements show near identical foam temperatures at 8.35 and 14.5 GHz, but large variations at 1.4 GHz. The resultant maximum foam emissivities at nadir range from 0.57 at 1.4 GHz to 0.84 at 14.5 GHz. The presence of the mono-molecular slick on the ocean surface had the same effect as a decrease in surface roughness. For horizontal polarization, the emission decreased below that of the surrounding ocean for all viewing angles. At vertical polarization, the emission decreased below and increased above a viewing angle of approximately 60 degrees. The change in temperature was observed at both 8.35 and 14.5 GHz, being barely detectable at 1.4 GHz.

1. INTRODUCTION

The dependence of the microwave brightness temperature on sea state and surface wind fields is under active investigation and has led to the prospect of remotely determining these parameters from a satellite on an all-weather basis. The usefulness of sea state and wind field data (in data scarce areas) would be of immense value to both meteorologists and oceanographers alike. Two oceanographic effects that play important roles in the dependence of the microwave signal on the sea surface are small-scale wave structure and foam.

The dependence of the observed microwave signal on sea surface structure manifests itself through the emission and reflection from dielectric media with all scales of surface roughness. These include not only the relatively smooth wind waves and swell much larger than the observing wavelength, but also the capillary and ultra-gravity waves present on the sea surface at low surface wind speeds. Current models of the sea surface include roughness both larger and smaller than the observing wavelength, but the effect of small-scale structure on the radiometric signal has yet to be experimentally verified.

Foam is a potentially more useful parameter to the remote sensing of the ocean surface by microwave radiometry. Beyond an initial start velocity of 7 m/sec, foam coverage increases with surface wind speed. The exact magnitude of the signal

increase depends on observing frequency, areal coverage of foam in the antenna beam and foam properties. Both the dependence of foam coverage with wind speed and the radiometric properties of foam are areas of active research. Of primary interest is the increase in temperature with frequency and the variation with viewing angle and polarization.

Experimental information about both of these phenomena has been obtained by the Naval Research Laboratory in a series of airborne multi-frequency radiometer measurements. In one set of observations, low altitude measurements were made of a surf-zone at a variety of viewing angles. In the other set, measurements were made of an ocean region in which the small-scale roughness had been suppressed by an artificial mono-molecular slick. This suppression enabled comparison to be made between an ocean surface having all scales of roughness present and one having just the large-scale structure.

## 2. INSTRUMENTATION

The measurements in these experiments were made with a three frequency, non-scanning, airborne radiometer system mounted on a NOAA C-130 aircraft. The antennas all have identical seven-degree beamwidths and were mounted on a hydraulically controlled platform that allowed viewing angles from nadir out to 80 degrees to be obtained. The antennas at  $K_u$  (14.5GHz) and X-band (8.35GHz) were horn-fed dielectric lenses while the L-band (1.4GHz) antenna was a dipole-fed eight foot diameter paraboloid. Periodic calibration of the radiometers was provided by noise diodes coupled into the reference arm of the radiometers. Simultaneous dual-polarization measurements were made at  $K_u$ - and X-band, while single polarization (either horizontal or vertical) was observed at L-band. Data were recorded both on analog strip-chart for instant monitoring purposes and also on magnetic tape for later digital processing. Sensitivity of the radiometers with a one second integration time was 0.21, 0.08 and 0.05 °K for L, X and  $K_u$ -bands respectively.

## 3. SLICK MEASUREMENTS

To determine the effect of small-scale roughness on the radiometric signal, one method is to suppress the small-scale waves in a specific area on the ocean surface. Although various types of oils damp small-scale waves, for sufficient oil thickness, oils have a radiometric effect of their own. This effect may overwhelm any change due to the damping of the small-scale structure. To eliminate this problem, oleyl alcohol was used for the experiment. It forms a mono-molecular slick on the ocean surface which is too thin to have a radiometric effect, yet damps out the capillary and ultra-gravity waves.

The oleyl alcohol was laid by the NOAA T-boat in the Atlantic Ocean about five miles from Miami, Florida. A total of nine passes along the length of the slick was made, with measurements being taken at angles from nadir out to 80 degrees. Based on laser geodilite data, the significant wave height was about 2.4 meters. Surface winds were 8 meters/sec, sufficient to produce some foam patches on the sea surface. Corresponding 35-mm photographs of the sea surface at a rate of one per second were used to confirm the areal extent of the slick.

The radiometer outputs as a function of time for a viewing angle of zero degrees are shown for horizontal polarization in Fig. 1 and vertical polarization in Fig. 2. The slick appears as a 2° K decrease in antenna temperature at both X- and  $K_u$ -bands and for both polarizations, with no detectable effect at L-band. The change in temperature with angle for both polarizations is summarized in Fig. 3 for  $K_u$ -band. The slick decreases the observed temperature for horizontal polarization at all angles, but produces an increase in temperature for vertical polarization near 80 degrees. Results obtained on 3 April 1973 under lighter sea state conditions are similar, but with a slight decrease in magnitude. The results for both days are summarized in Figs. 4 and 5, which show the temperature difference between polarizations due to the slick as a function of viewing angle. The difference between polarizations increases with increasing viewing angle and shows a slightly larger effect at  $K_u$ - than X-band. Surface roughness thus has little influence on the temperature change due to the slick until large viewing angles are obtained.

## 4. FOAM MEASUREMENTS

To investigate the radiometric properties of foam as a function of frequency and polarization, it is essential that the foam be identical in each case. This

was accomplished in the field observations by making measurements simultaneously at three frequencies and at both horizontal and vertical polarization at X- and K<sub>u</sub>-band. By using identical seven degree beamwidths for all antennas, different foam coverages among beams are eliminated and comparison can then be made. To obtain good foam coverage and sufficiently thick foam, observations were conducted parallel to a surf-zone. The measurements were made from an altitude of 150 meters at angles from nadir out to 53 degrees.

Figures 6 and 7 show the radiometer output as a function of time for all of the radiometers at a viewing angle of 28 degrees. The wide variations in signal are due to both variations in foam properties and foam coverage. One can notice the correlation between the three frequencies and both polarizations, with only a difference in magnitude. To illustrate the response between the different frequencies, Figs. 8 and 9 show scatter diagrams of the temperature increase due to the foam at L- and X-bands plotted against the increase at K<sub>u</sub>-band. The increase in all cases is the increase in brightness temperature above that from a specular surface. The linear relationship between X- and K<sub>u</sub>-bands compared to the variability at L-band indicates that the foam was sufficiently thick to have the same response at the higher frequencies, but variable response at L-band.

The results for all viewing angles are summarized in Fig. 10, which shows the maximum foam emissivity at K<sub>u</sub>-band as a function of viewing angle for both polarizations. The results at X- and L-band are not shown as the X-band values are within 1% of those at K<sub>u</sub>-band and those at L-band are similar in shape, only decreased in magnitude. For comparison purposes, the empirical model as put forth by Stogryn is also shown for the same conditions as the experiment.

The maximum value of the experimental emissivity at nadir is 0.84, less than the theoretical maximum of 1.0 for a perfect emitter. The results for all of the frequencies are shown in Fig. 11, which shows the observed foam emissivities as a function of frequency for nadir viewing angle. The empirical model of Stogryn is again shown for comparison. One important feature is the increase in emissivity of foam from L- to X-band and the flatness of the curve from X- to K<sub>u</sub>-band.

### 5. CONCLUSIONS

The absence of small-scale waves on the ocean surface changes the microwave emission at 8.35 and 14.5 GHz, and has a barely detectable effect at 1.4 GHz. At horizontal polarization, the change in emission is observed as a decrease in signal for all viewing angles. For vertical polarization, there is a decrease in emission for angles less than 60 degrees and an increase in signal beyond. The magnitude of the change in emission increases with increasing surface roughness, particularly for vertical polarization at large viewing angles. The measurements show that the sea surface becomes effectively smoother when the small-scale waves are damped, in that they have an exact opposite effect to an increase in surface roughness. Further experiments are required to determine whether the increase in emission from small-scale roughness is independent of the underlying large-scale roughness, or whether small-scale waves become important only after large-scale roughness is present. In any case, it is evident that small-scale roughness is important to the emission from the sea surface and must be included in any theoretical model.

The presence of foam on the sea surface is responsible for large increases in microwave emission at all of the frequencies investigated. The emission varies with areal coverage and foam properties, but is less at 1.4 GHz than at the higher frequencies. The variability at L-band is caused primarily by variations in foam depth, which are more important at the longer wavelengths. The emission from the foam is less than from a perfect emitter, but it is within 16% of that value at 14.5 GHz. For the thick foam of this experiment, the emissivity of foam increases gradually from 1.4 to 8.35 GHz, with negligible increase from 8.35 to 14.5 GHz. In general, the observed foam emissivities disagree with the empirical model of Stogryn, being up to 20 % greater in magnitude than his model.

For the conditions of this experiment, where relatively thick foam was observed the frequency dependence occurs between L- and X-band. More experimental work is required to determine if this frequency dependence holds in general. It is unlikely that the emissivity of foam would have the same frequency dependence or magnitude for the foam patches and streaks on the sea surface during high wind conditions. For the thinner foam patches and streaks, the change in emissivity would most likely occur at higher frequencies.

ORIGINAL PAGE IS  
OF POOR QUALITY

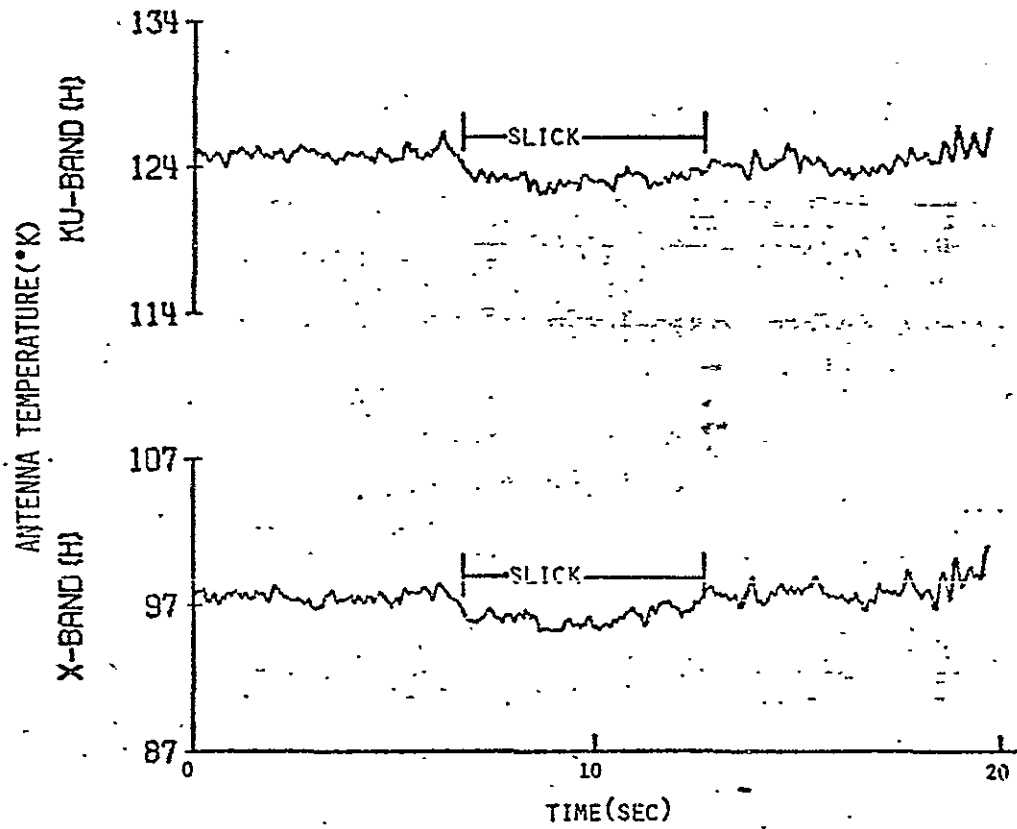


FIGURE 1. ANTENNA TEMPERATURES ALONG SLICK. Horizontal polarization, Frequencies = 8.35 and 14.5 GHz, Viewing angle = 0°, 11 April 1973.

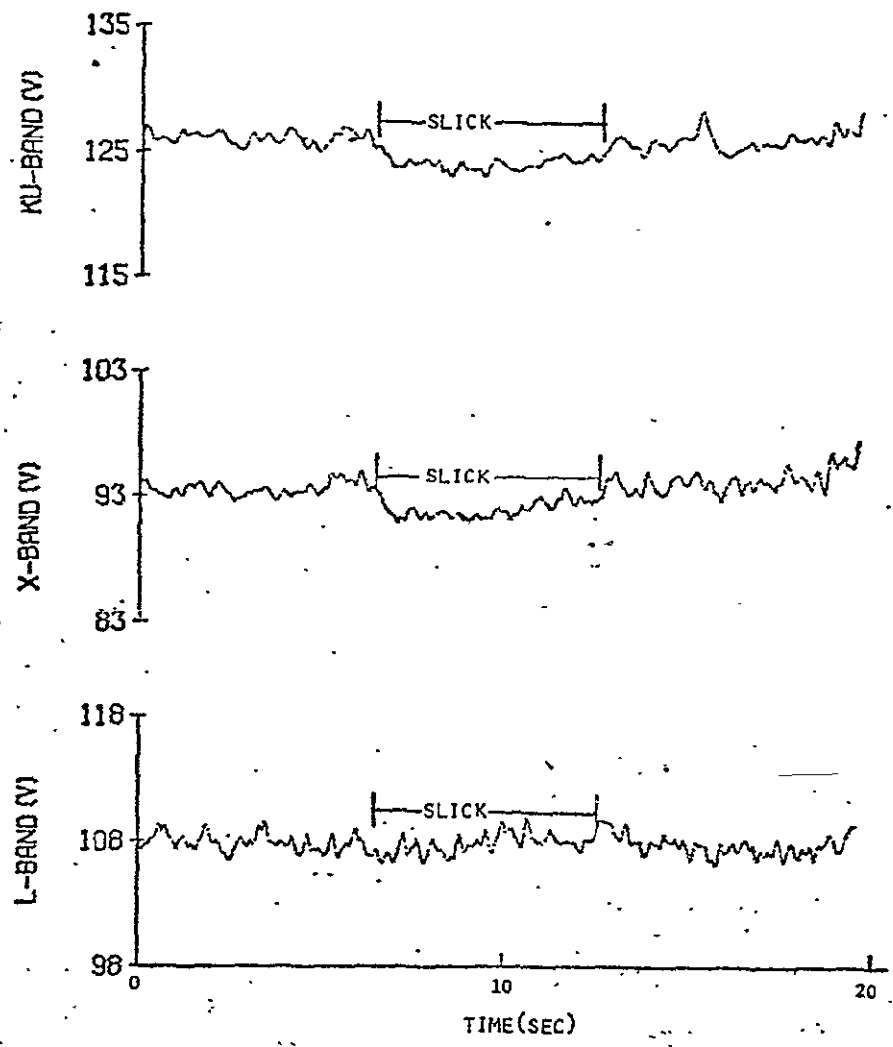


FIGURE 2. ANTENNA TEMPERATURES ALONG SLICK. Vertical polarization, Frequencies = 1.4, 8.35 and 14.5 GHz, Viewing angle = 0°, 11 April 1973.

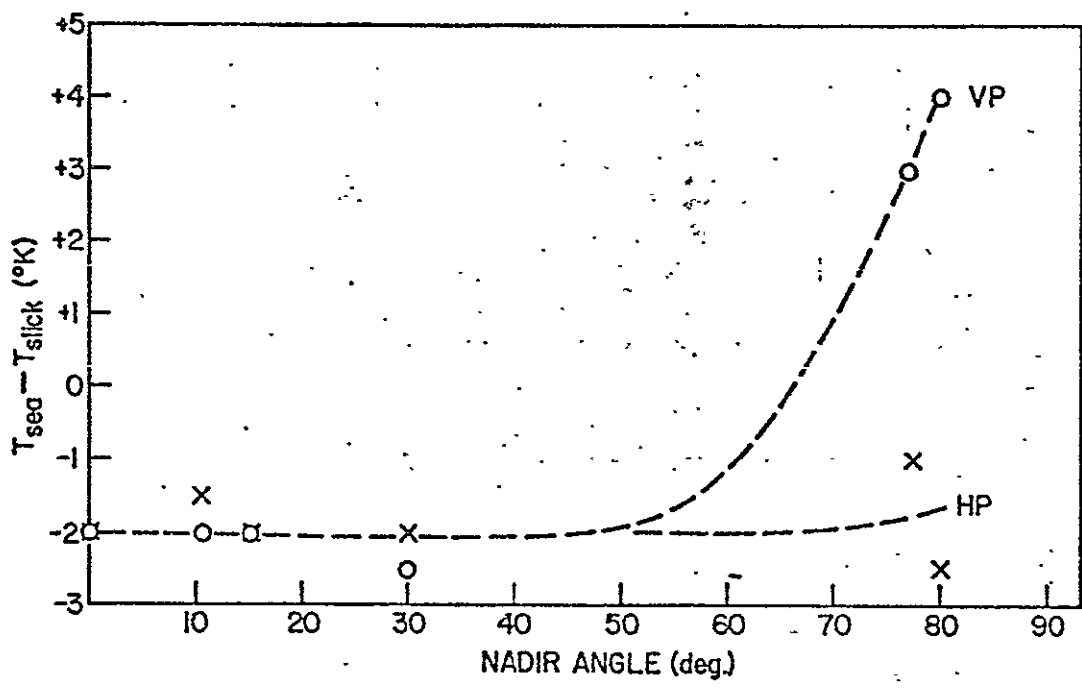


FIGURE 3. ANTENNA TEMPERATURE CHANGE DUE TO SLICK VERSUS VIEWING ANGLE. Horizontal and vertical polarization, Frequency = 14.5 GHz, 11 April 1973.

ORIGINAL PAGE IS  
OF POOR QUALITY

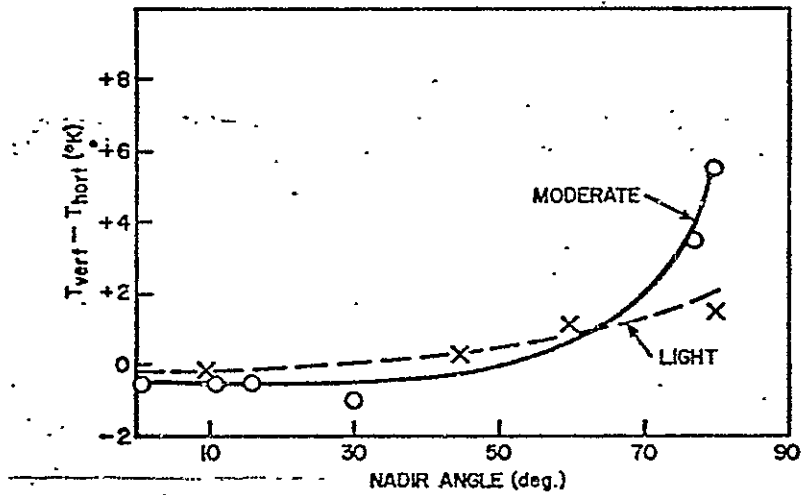


FIGURE 4. ANTENNA TEMPERATURE DIFFERENCE BETWEEN POLARIZATIONS VERSUS VIEWING ANGLE. Light and moderate surface roughness, Frequency = 8.35 GHz, 3 and 11 April 1973.

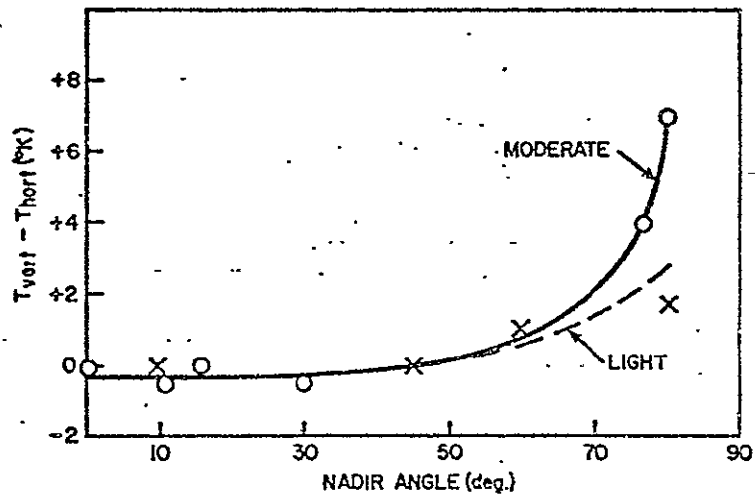


FIGURE 5. ANTENNA TEMPERATURE DIFFERENCE BETWEEN POLARIZATIONS VERSUS VIEWING ANGLE. Light and moderate surface roughness, Frequency = 14.5 GHz, 3 and 11 April 1973.

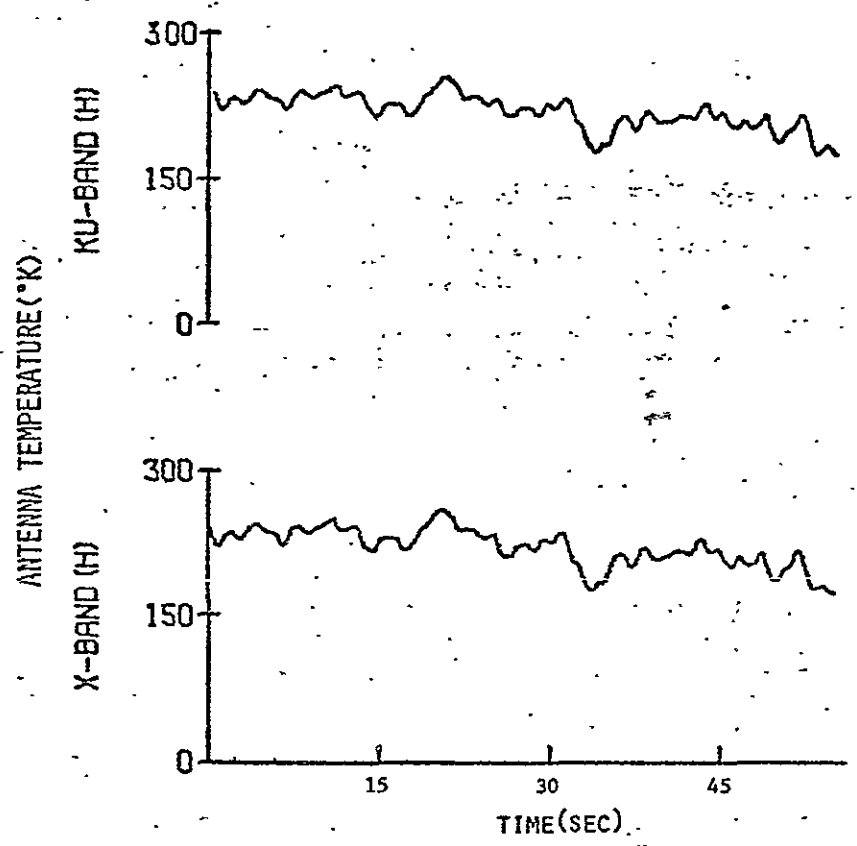


FIGURE 6. ANTENNA TEMPERATURES ALONG SURF-ZONE.  
Horizontal polarization, Frequencies = 8.35 and  
14.5 GHz, Viewing angle = 28°, 6 June 1973.

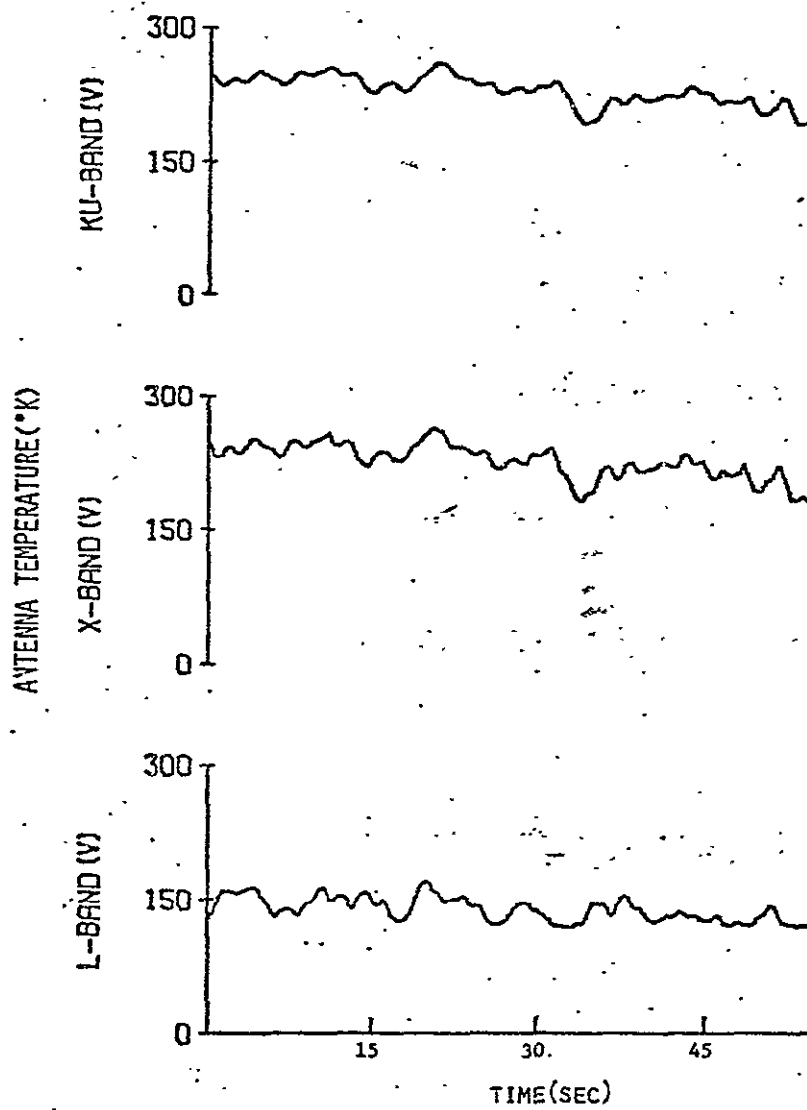


FIGURE 7. ANTENNA TEMPERATURES ALONG SURF-ZONE.  
Vertical polarization. Frequencies = 1.4, 8.35  
and 14.5 GHz, Viewing angle = 28°. 6 June 1973.

ORIGINAL PAGE IS  
OF POOR QUALITY

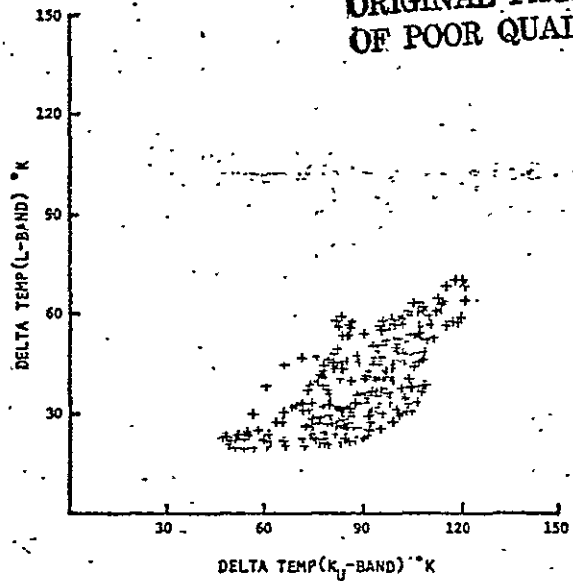


FIGURE 8. SCATTER DIAGRAM OF TEMPERATURE INCREASE DUE TO FOAM AT L- AND  $K_u$ -BANDS. Vertical polarization, Viewing angle =  $28^\circ$ , 6 June 1973.

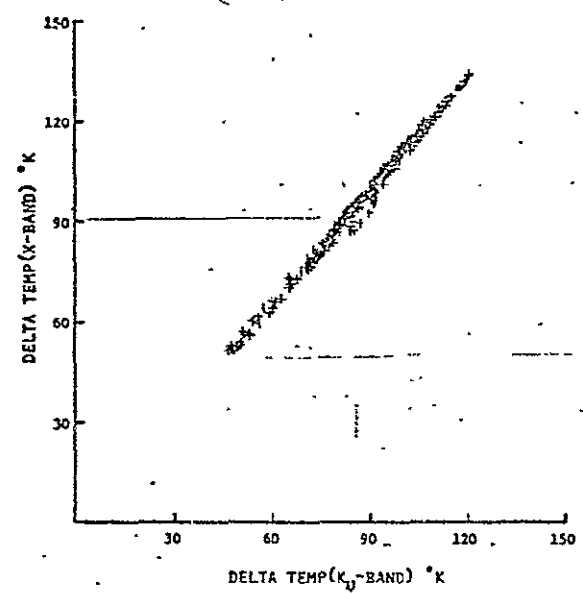


FIGURE 9. SCATTER DIAGRAM OF TEMPERATURE INCREASE DUE TO FOAM AT X- AND  $K_u$ -BANDS. Vertical polarization, Viewing angle =  $28^\circ$ , 6 June 1973.

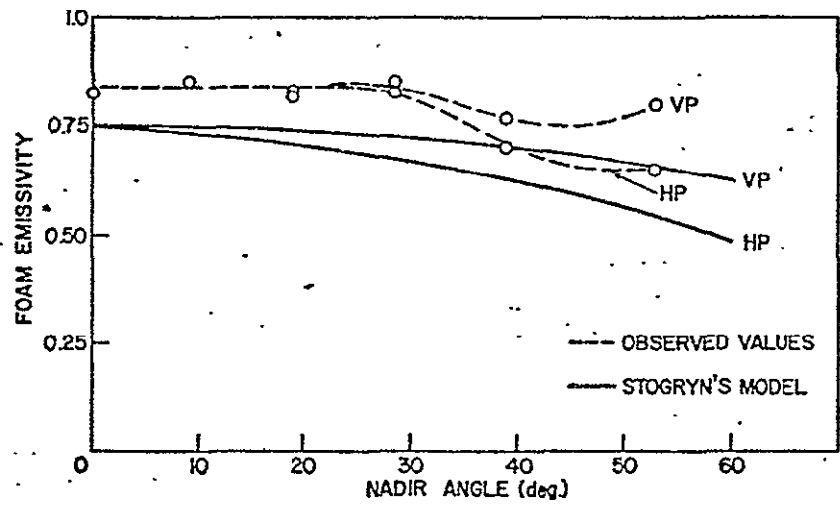


FIGURE 10. EMISSIVITY OF FOAM VERSUS VIEWING ANGLE. Horizontal and vertical polarization, Frequency = 14.5 GHz, 6 June 1973.

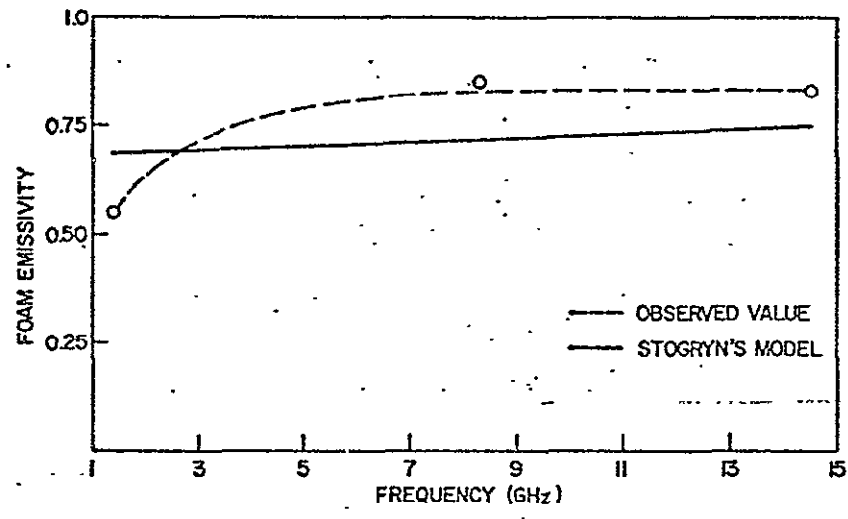


FIGURE 11. EMISSIVITY OF FOAM VERSUS FREQUENCY. Viewing angle = 0°, 6 June 1973.

ORIGINAL PAGE IS  
OF POOR QUALITY  
1773

## Appendix B

ORIGINAL PAGE IS  
OF POOR QUALITYA REMOTE SENSING STUDY OF PACIFIC HURRICANE AVA

D. Ross

National Oceanic and Atmospheric Administration  
Miami, Florida

B. Au

Naval Research Laboratory  
Washington, D. C.

W. Brown

Jet Propulsion Laboratory  
Pasadena, California

J. McFadden

National Oceanic and Atmospheric Administration  
Miami, Florida

## ABSTRACT

Aircraft, SKYLAB, NOAA-2, ATS-3, and NIMBUS-5 recently obtained a variety of measurements of Pacific Hurricane AVA. These measurements are unusually broad in scope and include satellite observed passive microwave emissivities at 13.9 + 19.5 GHz, active microwave scattering cross-sections at 13.9 GHz, and near infrared and visible images. Essentially simultaneous aircraft measurements of wind speed, waves, whitecaps, 1.4 and 13-15 GHz passive microwave emissivities, 1.4 GHz active microwave images, sea surface temperatures, pressure fields, and aerosol size distributions were also obtained. A brief description of sensors and platforms is presented along with some in-depth details of results obtained. These results confirm the sensitivity of microwave emissivity to foam and liquid water in the atmosphere. Wave measurements from the aircraft show significant differences in the shape of the energy spectrum when compared to other fetch-limited spectra. Whereas fetch-limited spectra are sharply peaked, the hurricane spectra remote from the eye are broad, indicating the presence of swell and increased energy transfer within the spectrum due possibly to non-linear interactions, while those near the eye are sharply peaked.

The SKYLAB RADSCAT, operating at 13.9 GHz in a cross-track mode, obtained microwave measurements of a portion of the storm in both the active and the passive mode. Preliminary results show that the scattering cross-sections increase when viewing the hurricane despite an expected attenuation due to rain. Passive measurements increase as expected and are in general agreement with NIMBUS-5 measurements at 19.5 GHz.

Aircraft measurements of microwave brightness temperatures at L band show an increase which is

largely due to foam and whitecaps while those at X and KU band are contaminated by rain. Active coherent L-band radar images of swell produced by the hurricane were obtained enroute to the storm. These images indicate a strong interaction takes place between long and short gravity waves.

Flight level wind speeds were obtained by means of an inertial navigation system and represent a significant increase in accuracy from past measurements of hurricane winds. Maximum winds encountered in the eye wall measured 137 knots, the highest ever for a Pacific hurricane, which had a record low central pressure of 914 mb.

The use of extensive and coordinated satellite and aircraft measurements has provided an unprecedented opportunity to study the dynamics of a hurricane.

## 1. INTRODUCTION

The development and application of remote sensing techniques to the study of man's environment has increased considerably in recent years. Perhaps the greatest return on monies invested in this area has been in use of satellites in observing and predicting weather. One aspect of weather phenomena which is currently being studied in great detail is tropical cyclones. A tropical cyclone is an intense vortex of high winds and large moisture concentrations which can have a devastating effect on man as they pass from water to land accompanied by high wind forces, inordinately high water (surge) levels, and large amounts of rain. Because cyclones are generally born in remote ocean areas, they have remained a little understood phenomena. In recent years, however, aircraft have been used to study many aspects of the storms by means of a variety of in-situ measurements. More recently, satellites equipped with imaging systems have been of great utility in detecting the birth of cyclones and predicting the path they are most likely to follow during their lifetime.

This paper describes a number of measurements of some unique aspects of a cyclone obtained from aircraft and a variety of spacecraft and represents an unprecedented opportunity to evaluate the capability of remote sensing instrumentation to contribute to the study of such phenomena.

## 2. BACKGROUND

The NASA SKYLAB experimental satellite was the catalyst needed to get this experiment. Intended as a means of evaluating the Radar-Radiometer sensor packages aboard SKYLAB, an aircraft program was initiated to fly beneath the SKYLAB and measure an extensive number of environmental parameters which might affect the signature of the earth viewing satellite sensors. One of the aircraft involved was a National Oceanic and Atmospheric Administration (NOAA) C130 Hercules normally equipped to study hurricanes and other weather-oriented phenomena. For the SKYLAB program, a number of additional sensors were installed and are shown in Table I along with the parameter intended to be studied and expected accuracy. Figure 1 shows the NOAA aircraft with passive microwave radiometers extended out the rear cargo door.

As the NOAA SKYLAB underflight program was getting underway, the first Pacific Hurricane of the season was forming and was named AVA, (Figure 2). As one of the objectives of the SKYLAB program was to observe hurricanes, a data gathering pass was planned for 6 June 1973, using the SL 193 Radar-Radiometer in the solar inertial scanning mode. Unfortunately, a more extensive look at the hurricane with other SKYLAB sensors could not be arranged because of conflicting priorities. Indeed, the NASA system was literally turned upside down in order to schedule this limited pass.

## 3. AIRCRAFT MEASUREMENTS

The NOAA C130 deployed to Acapulco the morning of 6 June, refueled and commenced its flight into the storm at 2107Z. Figure 3 shows the track of the aircraft along with isolines of flight level (500 ft.) winds measured with a Litton LTN-51 inertial system using the true airspeed output from a Kollsman differential pressure transducer. As a result of a measurement of an extraordinarily low central pressure of 915 mb obtained by an Air Force Reconnaissance aircraft approximately three hours prior to our entry into the storm, it was decided a low level (500 ft.) penetration into the eye would be unwise. The portion of the track shown in Figure 3 from 2156 to 2315 was therefore flown at 10,000 feet. Low level (500 ft.) measurements of wind speed and direction, wave heights, whitecap densities, and microwave emissivities were obtained during the period 2107-2156, and again from 2325 to 2356. Microwave measurements, which require the cargo door to be open with extended radiometers, were not taken during the latter time period because of the reduced safety factor associated with high turbulence in conjunction with open cargo doors.

Figure 4 is an example of laser altimeter profiles of waves in an area of 65 knot flight level winds. Figure 5c shows the spectra of this segment, mapped to fixed coordinates, along with a spectra of high waves measured in the North Sea (Ross, et al., 1970). Also shown are spectra (Panel a, b) obtained at other regions within the storm plotted together with spectra of the same total energy obtained in the N-Sea and the North Atlantic. There are some significant differences between these sets of spectra. Those obtained near the eye (Fig. 5b, c) are sharply peaked and agree well with the N-Sea spectra which are severely fetch limited. The third spectrum was obtained approximately 110 nautical miles from the eye and shows considerably more low frequency energy than the North Atlantic spectrum which was essentially fully developed. In addition, this spectrum shows a reduced level of energy on the high frequency side of the peak. We attribute this difference to non-linear interactions between the high frequencies and swell of frequencies near the peak which results in a broadening of the hurricane spectrum. Figure 6 shows the variation of wind speed and significant wave height with radial distance from the eye. The dashed line shows expected surface (20 meter) winds assuming a logarithmic variation in wind between the surface and flight altitude (Cardone, 1969). The significant wave height is known to vary as the square of the wind speed for fully developed seas. It can be seen in this figure that this relationship does not hold in a hurricane because of the fetch and duration limited character of the hurricane wind field.

Observations of microwave brightness temperature were obtained during the period 2107-2147. The data at the higher microwave frequencies are strongly affected by the presence of rain as one-minute average values at vertical incidence vary inconsistently from  $130^{\circ}$  to  $145^{\circ}$ , and  $140^{\circ}$  to  $200^{\circ}$  for X and KU Band respectively. Brightness temperature vs. incidence angle for this segment at L-Band is shown in Figure 7 along with data for a low wind condition obtained 11 June. It can be seen that there is a systematic increase in brightness temperatures of about  $4^{\circ}\text{K}$  at all incidence angles. Inspection of simultaneous vertical photography reveals little thin foam streaking presumably because of the swell content of the seaway and the percentage of whitecap coverage is approximately 10 percent. Based on the results of Au, et al. (1974), presented elsewhere in this symposium, we attribute this increase to the whitecap (foam) coverage. Thus, a sensitivity of  $.4^{\circ}\text{K}/\%$  whitecap coverage is obtained.

Enroute to the storm, coherent side-looking radar operating at a frequency of 1.35 GHz ( $\lambda = 25$  cm) was used to obtain surface imagery. A series of wave-like patterns is apparent in this imagery which appears to be a combination of locally generated wind waves mixed with swell coming from the hurricane. This imagery, together with a vertical photograph obtained simultaneously, was digitized and subjected to two-dimensional Fourier analysis. Figure 8 shows the optical image of the two-dimensional Fourier transform at the top, along with a densitometer trace obtained along the axis of the principal direction (lower left, and center). Also shown is a composite hindcast wave spectrum constructed by using the wave spectra obtained at 2147Z along with a spectrum obtained in the Atlantic Ocean for a wind speed of approximately 22 knots. Surface winds at the time of this image were visually estimated to be 20 knots, which was substantiated by sun glint analysis of ATS-3 Satellite imagery (Strong, 1973). The position of the laser wave measurements and of the hurricane relative to the radar imagery is shown in the inset in

the upper right corner of the figure. Good agreement between the wave lengths of the principal wave components can be seen. That the radar is imaging the waves is evident; not so evident is the scattering mechanism which allows detection of waves longer than the backscattering Bragg waves (Crombie, 1955). It has been demonstrated in several laboratory and field experiments (cf. Shemdin, et al., 1972, Mitsuyasu (1971)) that presence of a swell in a wind sea will reduce the amplitude of the wind-wave energy peak by an amount which is dependent upon the energy and frequency separation of the swell. Longuet-Higgins (1969) describes this interaction which results in shorter waves peaking near the crest of the longer wave as it passes by. The long waves thus modulate the Bragg waves which, in turn, modulate the return of the radar energy resulting in an image of the longer waves. Since more than one long wave component is seen in the image, it has been suggested (Stilwell, 1974) that this modulation is accomplished by interaction between all waves longer than the Bragg waves. The radar imagery therefore may contain useful amplitude as well as wave length and direction information if the transfer function for the former can be established. Unfortunately, the radar power supply gave out shortly after this segment was completed so that no imagery of the local hurricane wave field was obtained during the eye penetration.

#### 4. SATELLITE RESULTS

Imagery and microwave data from a variety of satellites were obtained of the hurricane in various stages of development. A summary of these satellite studies is shown in Table II. Figure 9 is a composite of ATS imagery showing the track of SKYLAB as it passed near the storm. Unfortunately, the storm was moving rather fast, and although the SKYLAB antenna scanned to 52° incidence angle, only a small portion of data was obtained in the high wind periphery of the storm. This data, along with NIMBUS 19.5 GHz measurements of the same portion of the storm, are shown in Figure 9 for the incidence angles of 45° to 52.5°. Also shown are rainfall rates inferred from the 19.5 GHz NIMBUS-5 radiometer (Wilheit, 1974).

The purpose of the S 193 Radar-Radiometer is to infer surface wind fields from measurements of the microwave backscatter. The passive portion of the instrument is intended to provide a basis for correcting the return radar cross-section ( $\sigma^0$ ) due to attenuation by liquid water. The inference of surface wind speed is further complicated because the amplitude of the backscattered component is sensitive to the relative direction of the wind vector. Jones (1974), from data obtained with an aircraft system at vertical polarization, reports a difference of about 5 db between the upwind and cross-wind directions for a wind speed of 14 m/s and incidence angle of 40°, vertical polarization. The up-downwind asymmetry he observed of 1-2 db is further evidence of short wave modulation by longer waves. Estimates of wind direction along the footprint were made as previously described and resulted in positive corrections of 2-4 db. A backscattered component due to rainfall is not accounted for in the data which are summarized in Table III.

It can be seen from panel a of Figure 10 that if a correction were applied to  $\sigma^0$  values, due to rain attenuation, that the  $\sigma^0$  for both polarizations would increase with increasing wind speed between 1857:15 and 1858:00. Neglecting the value at 1858:16,  $\sigma^0$  would then decrease at 1858:31, following the decreasing trend in surface wind. At the 45° incidence angle (panel b), rainfall rates were markedly reduced and  $\sigma^0$  qualitatively agrees with trends in the wind speed.  $\sigma_{VV}^0$ , in both cases, has been corrected for wind direction while no such correction has been applied to  $\sigma_{HH}^0$ . As with the coherent radar images, the  $\sigma^0$  is a measure of the energy content of resonant Bragg waves - near capillary, or centimeter, wavelengths in the case of the S 193 radar. Phillips (1966) using dimensional arguments shows that the high frequency end ( $f_i > f_m$ )\* of the gravity wave spectrum should reach a maximum, or equilibrium, value. Increased energy transfer into this spectral region would simply result in increased energy loss through wave breaking. Pierson and Stacy (1973) suggest three forms for the behavior of the high frequency end of the spectrum, including the ultra-gravity and capillary regions, which are wind speed dependent and result in increased wave energy levels for all increasing winds. Hasselmann, et al. (1973), show that the Phillips equilibrium constant decreases with increasing fetch indicating long wave-short wave interaction is important in the behavior of the high frequency tail of the spectrum.

---

\* $f_m$  is the frequency at which the peak energy occurs.

From the observations of SKYLAB measurements obtained in Hurricane AVA, it is tempting to attribute the observed  $\sigma^0$  variations to corresponding variations in energy level of wind speed dependent Bragg waves. On the basis of this limited data set, the considerable potential for errors associated with the corrections required for attenuation, relative wind direction, and backscatter due to rain, and an unknown sensitivity of  $\sigma^0$  at high wind speeds, we reject this step at this particular time. A final conclusion must await additional data obtained for high sea states during SL4 and a better estimate of azimuth dependence of  $\sigma^0$  for different wind speeds and both polarizations.

## 5. CONCLUSIONS

It can be concluded from this data set that the use of remote sensors could be a useful tool in the monitoring and study of tropical cyclones. The potential for such sensors listed by observational category is as follows:

1. Active microwave - Both cross-sectional as well as imaging microwave systems can be used to map aspects of the wave field of a hurricane. High frequency systems, such as the SKYLAB RADSCAT, may have reduced utility in areas of heavy rain, while low frequency imaging systems will be limited primarily by the required high data rates.
2. Passive microwave - Aircraft and satellite measurements at 1.4, 8.35, 14, and 19.5 GHz show the higher frequencies to be capable of determining liquid moisture budget while the lower frequencies could be useful for determining the atmosphere-ocean energy exchange budget because of a sensitivity to energy loss occurring through the wave spectrum. However, because of diminished sensitivity at 1.4 GHz, a frequency somewhat higher, but less than 6 GHz, would be more appropriate.
3. Visible:
  - a. Satellites - Visible region imagery has been extremely useful in positioning the hurricane, calculating its forward velocity, and estimating the degree of asymmetry of the hurricane.
  - b. Coherent - Red laser light can be used with good results from low aircraft altitudes to profile surface waves despite heavy rain and spray, and the wave measurements can be used to bound the role of momentum transport to the ocean.
  - c. Photographic - Observations of whitecap density, which is related to momentum transfer and the wave spectrum, can be obtained. Thin foam streak direction relative to the eye of the hurricane could give an estimate of inflow angle of the surface winds.

## ACKNOWLEDGMENTS

The authors are indebted to the many people from different organizations who participated in the gathering of this data, especially the crew of SKYLAB and the NOAA CL30.

The personal efforts of Professors Willard Pierson and Richard Moore, and Messrs. Zack Byrns, Dean Morris, and Anthony Calio of NASA, JSC, and others who contributed to the rearrangement of the SKYLAB work schedule required to launch this experiment are recognized and thoroughly appreciated.

## REFERENCES

- Au, B., J. Kenney, L. U. Martin, D. B. Ross, Multi-frequency radiometric measurements of foam and a mono-molecular slick, Proceedings of the Symposium on Remote Sensing of Environment, Willow Run Laboratories, Ann Arbor, Michigan, 1974.
- Cardone, V. J., Specification of the wind field distribution in the marine boundary layer for wave forecasting, Rep. TR 69-1, Geophys. Sci. Lab., New York Univ., New York, December, 1969.
- Crombie, D. D., Doppler spectrum of sea-echo at 13.56 mc/s, Nature, 175, 681-682, 1955.
- Hasselmann, et al., Measurements of wind-wave growth and swell decay during the Joint North Sea Wave Project (JONSWAP), Deut. Hydrogr. Z., Deutsches Hydrographisches Institut, Hamburg, FRG, 1973.
- Jones, W. Linwood, Personal communication, 1974.
- Longuet-Higgins, M. S., A nonlinear mechanism for the generation of sea waves, Proc. Roy. Soc. A., 311, 371-389, 1969.
- Mitsuyasu, H., R. Nakayama, T. Komori, Observations of wind and waves in Hakata Bay, Rep. Research Inst. Appl. Mech., Kyushu Univ., 19, 37-74, 1971.
- Phillips, O. M., The dynamics of the upper ocean, 261 pp., Cambridge University Press, London, 1966.
- Ross, D. B., and V. J. Cardone, Laser observations of wave growth and foam density for fetch-limited 17-25 m/s winds, IEEE Trans. Geosci. Electron., GE-8(4), 326-336, 1970.
- Shemdin, O. H., R. J. Lai, A. Reece, and G. Tober, Laboratory investigations of white-caps, spray, and capillary waves, Tech. Report No. 11, Coastal and Oceanographic Engineering Laboratory, Univ. of Florida, Gainesville, Florida, 1972.
- Strong, A., Personal communication, 1973.
- Stilwell, D., Personal communication, 1974.
- Wilheit, T., Personal communication, 1974.

ORIGINAL PAGE  
OF POOR QUALITY

ORIGINAL PAGE IS  
OF POOR QUALITY

TABLE I. NOAA C130 AIRCRAFT INSTRUMENTATION

Parameter	Instrument	Accuracy
Wind Speed/Direction	LTN-51 Inertial Navigation System	± 2.0 kts
Sea Surface Temperature	Barnes PRT-5	± 1.0°C
Microwave Emissivity	1.4, 8.5, 14 GHz Radiometers	± 1.0°K
Wave Heights and Lengths	Laser Altimeter	± 1% or 3"
Wave Length and Direction	Coherent Radar 1.35 GHz	± 10%
White Caps and Foam	35 mm Vertical Camera	± 20% of Observation
Liquid Water Content	Johnson Williams Hot-Wire	± 15%

TABLE II. SUMMARY OF SATELLITES USED TO STUDY HURRICANE AVA

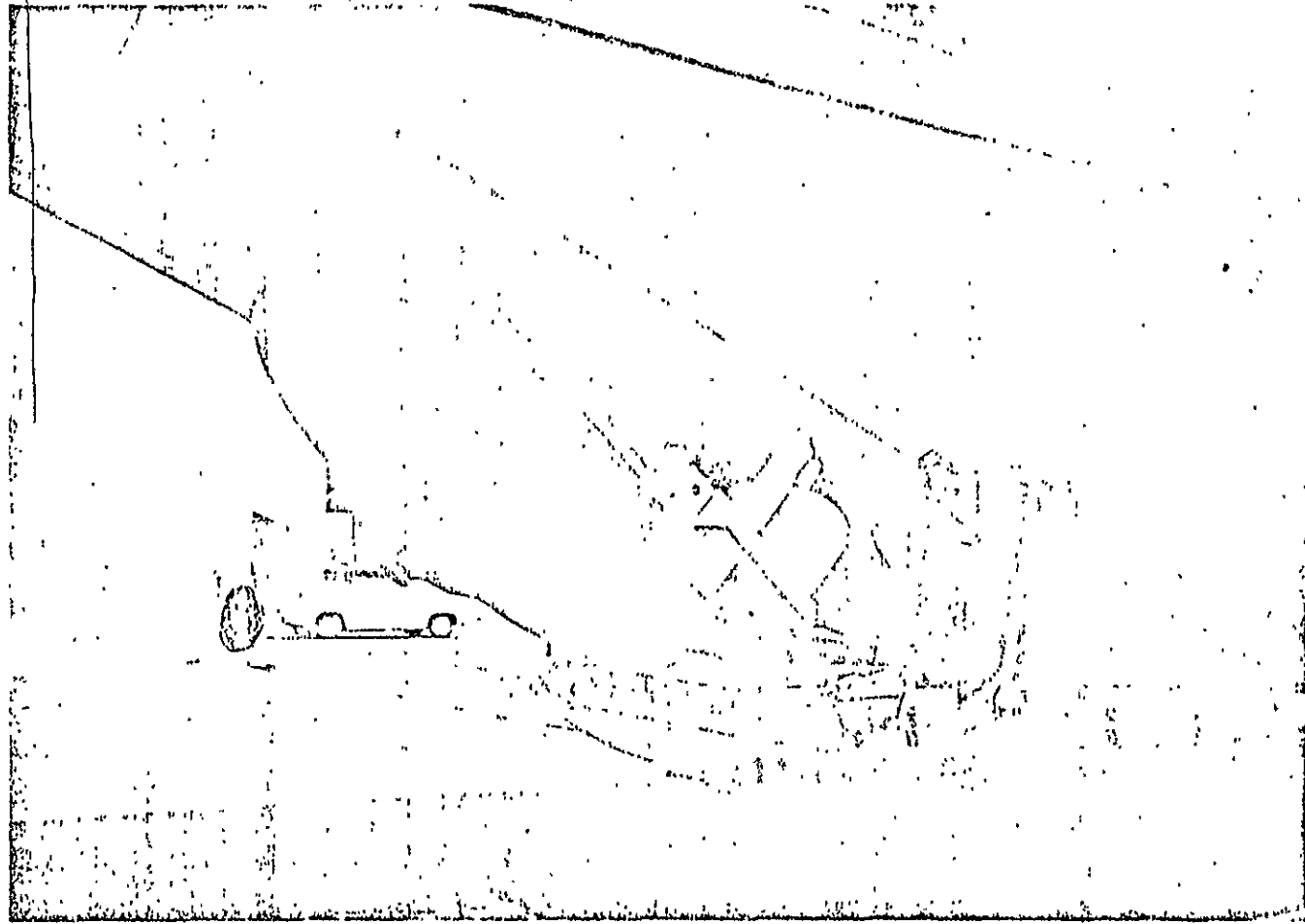
Satellite	Imagery Type	Microwave Data	Use
1. ATS	Visible	—	Positioning, Cloud cover
2. NIMBUS-5	Microwave	19.5 GHz HH, VV	Positioning, Rainfall rate
3. NOAA-2	Visible Infrared	—	Positioning, Asymmetry Cloud Cover
4. SKYLAB	Photography	13.5 GHz HH, VV HV, VH	Surface Winds Rainfall Distributions
5. DPP	Visible Infrared		Positioning, Cloud cover, Asymmetry Cloud Heights

TABLE III. SUMMARY OF SATELLITE OBSERVATIONS

SKYLAB Time	NIMBUS-5 19.5 GHz $T_{BH}$ (°K)	Rain- fall (mm/hr)	S193 $T_{HH}$ (°K)	S193 $T_{VV}$ (°K)	S193 <sub>0</sub> $\sigma_{VV}$ (db)	S193 <sub>0</sub> $\sigma_{HH}$ (db)	$\bar{U}_{20}$ (kts)	$\theta_U$ (Deg.)	Rela- tive Azi- muth (Deg.)	$\sigma_{VV}^0$ Cor- rec- tion (db)	S193 Inci- dence Angle (Deg.)
1857:15	170	2	121	173	-14	-19	36	90	150	+2	52.5
1857:30	170	2	124	174	-14	-20	42	90	150	+2	52.5
1857:45	193	25	145	188	-13	-16	48	120	120	+4	52.5
1858:00	193	25	152	189	-14	-15	40	160	80	+3	52.5
1858:16	200	50	216	233	-13	-13	39	160	80	+3	52.5
1858:31	180	5	135	185	-17	-19	32	160	80	+3	52.5
1857:18	170	2	122	161	-14	-17	32	90	150	+2	45.0
1857:34	170	2	122	161	-14.5	-19	36	90	150	+2	45.0
1857:49	170	2	140	175	-15	-16	36	110	130	+3	45.0
1858:04	175	3	136	171	-13	-16	37	140	100	+5	45.0
1858:20	182	6	128	165	-14.5	-18	36	120	120	+4	45.0
1858:35	180	5	132	169	-18.5	-21	28	100	100	+5	45.0

170

07



• 171

ORIGINAL PAGE IS  
OF POOR QUALITY

FIGURE 1. NOAA RESEARCH FLIGHT FACILITY C130 AIRCRAFT SHOWING 1.4 GHZ PASSIVE RADIOMETER IN THE VERTICAL INCIDENCE FLIGHT POSITION.

ORIGINAL PAGE IS  
OF POOR QUALITY.

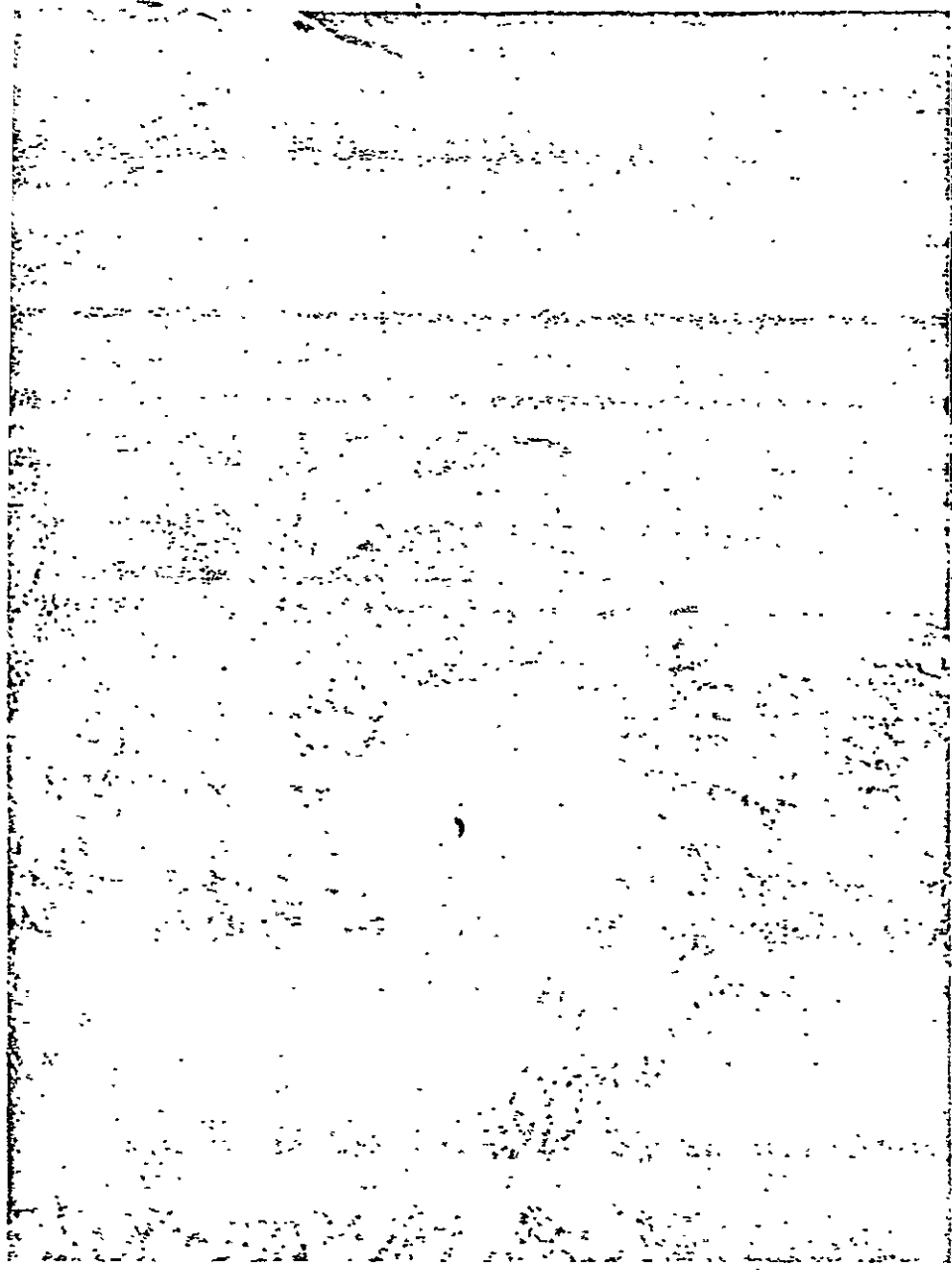


FIGURE 2. NOAA-2 VISIBLE REGION VIEW OF  
PACIFIC HURRICANE AVA ON 6 JUNE 1973.



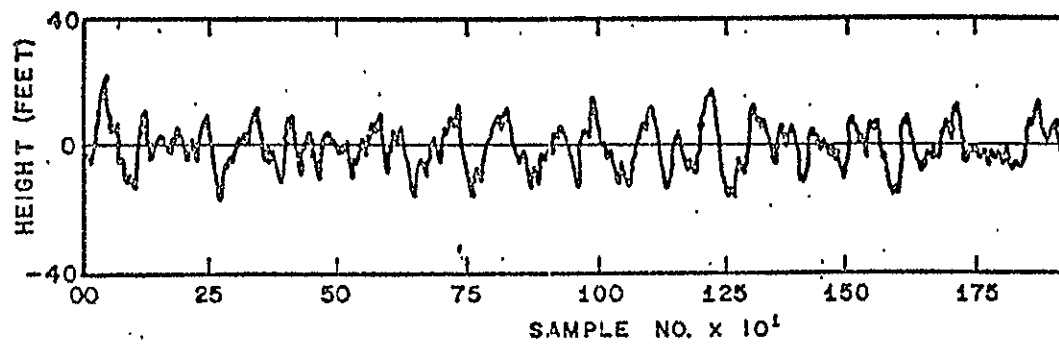


FIGURE 4. LASER MEASUREMENTS OF SURFACE WAVE CONDITIONS NEAR THE CENTER OF HURRICANE AVA. Flight level winds averaged for 1 minute were 6

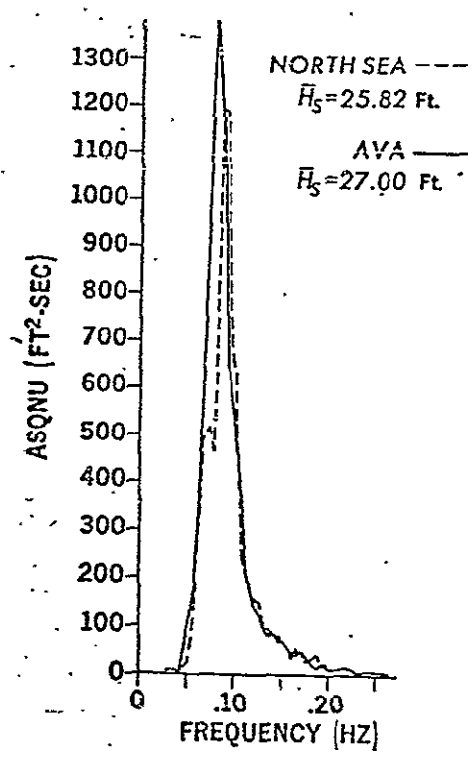
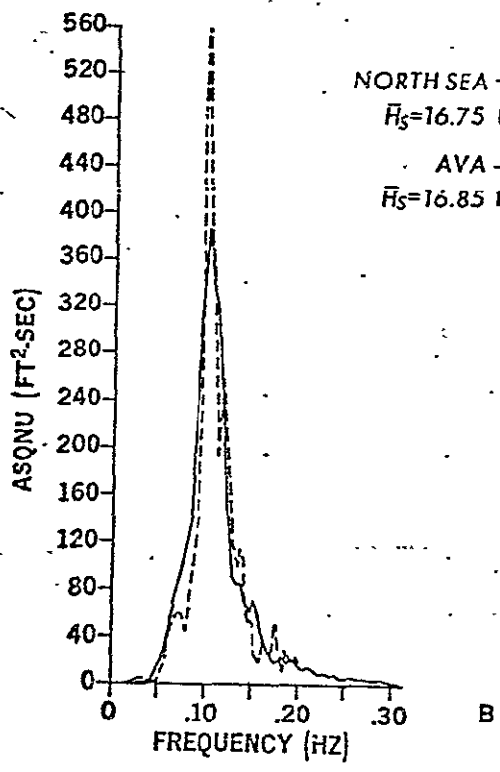
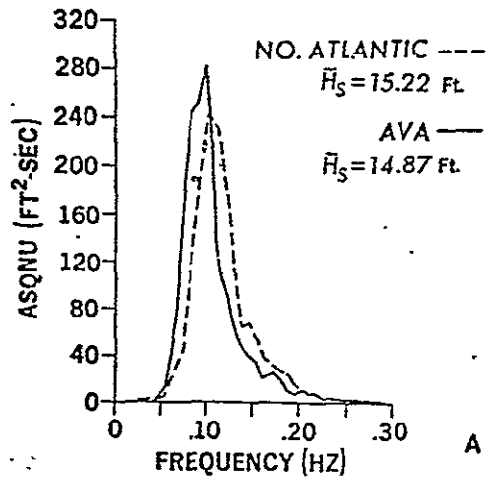


FIGURE 5. HURRICANE AVA WAVE SPECTRA COMPARED TO OTHER SPECTRA OF SIMILAR ENERGY CONTENT AND WIND SPEEDS.

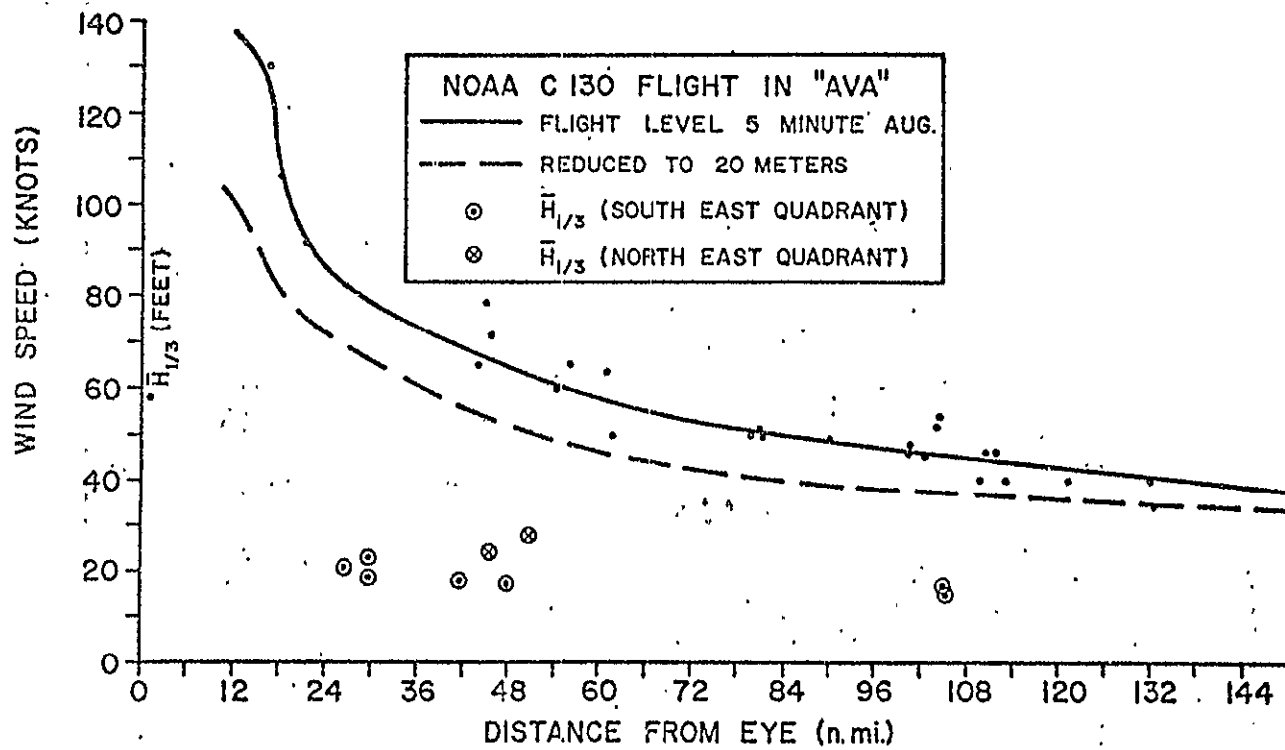


FIGURE 6. RADIAL PROFILE OF WIND SPEED AND SIGNIFICANT WAVE HEIGHT FOR PACIFIC HURRICANE AVA.

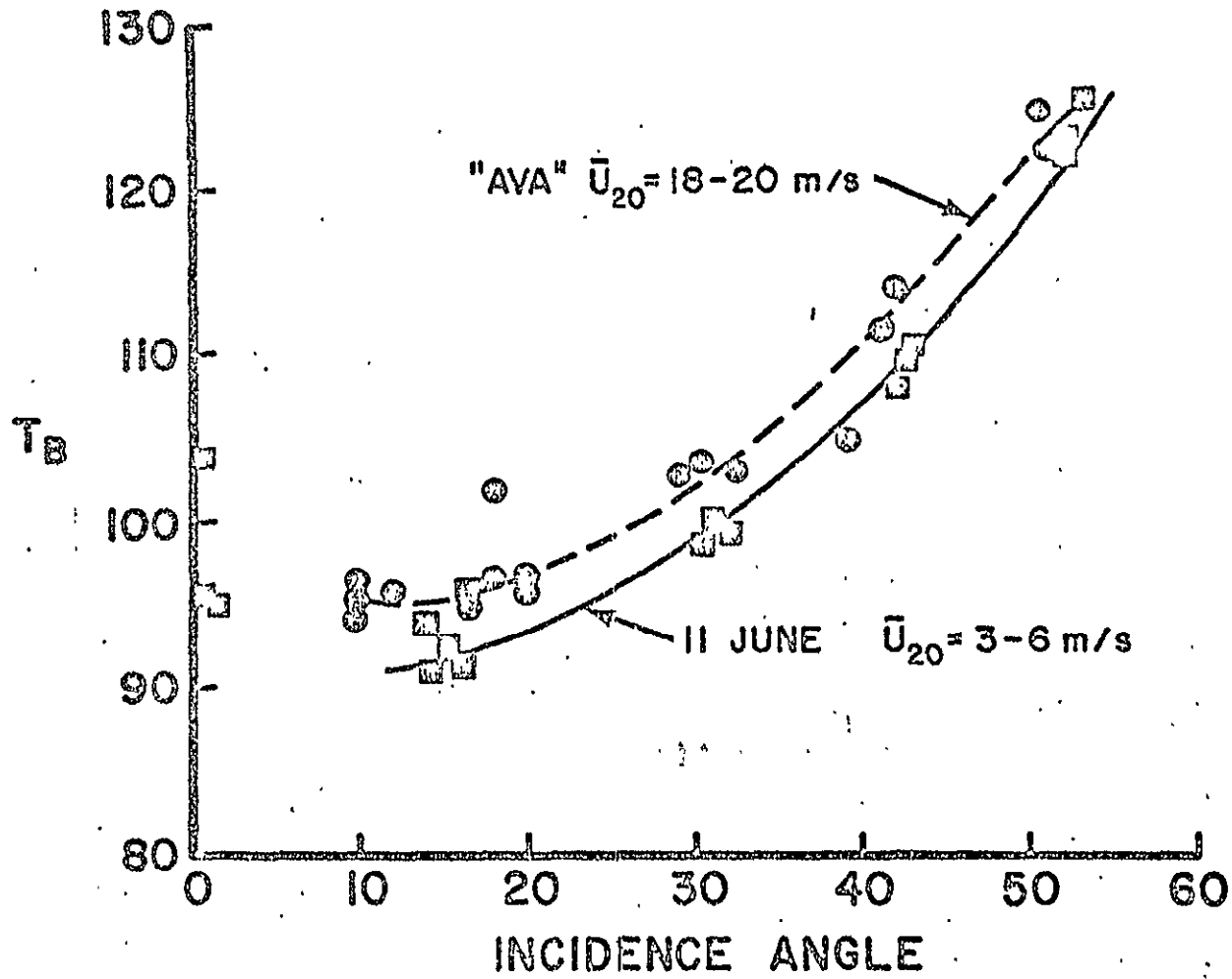


FIGURE 7. L-BAND VERTICALLY POLARIZED BRIGHTNESS TEMPERATURES FOR HURRICANE AVA AND LOW WIND CONDITIONS OF 11 JUNE.

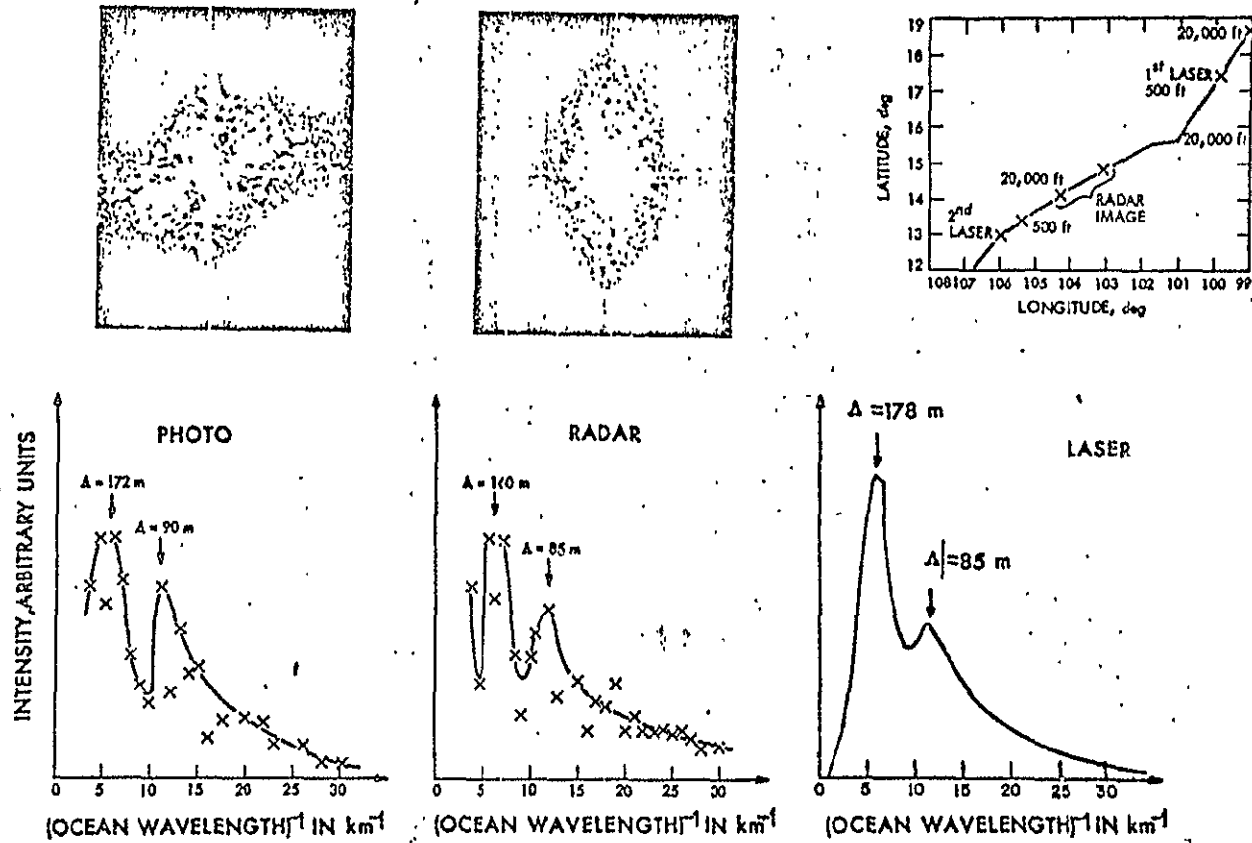


FIGURE 8. TWO-DIMENSIONAL FOURIER ANALYSIS OF COHERENT RADAR IMAGERY AND VERTICAL PHOTOGRAPHY OF HURRICANE AVA GENERATED WAVES COMPARED TO A COMPOSITE OF LASER WAVE MEASUREMENTS AT 13°N, 106°W AND FOR A FULLY DEVELOPED 11 M/S WIND SPEED.

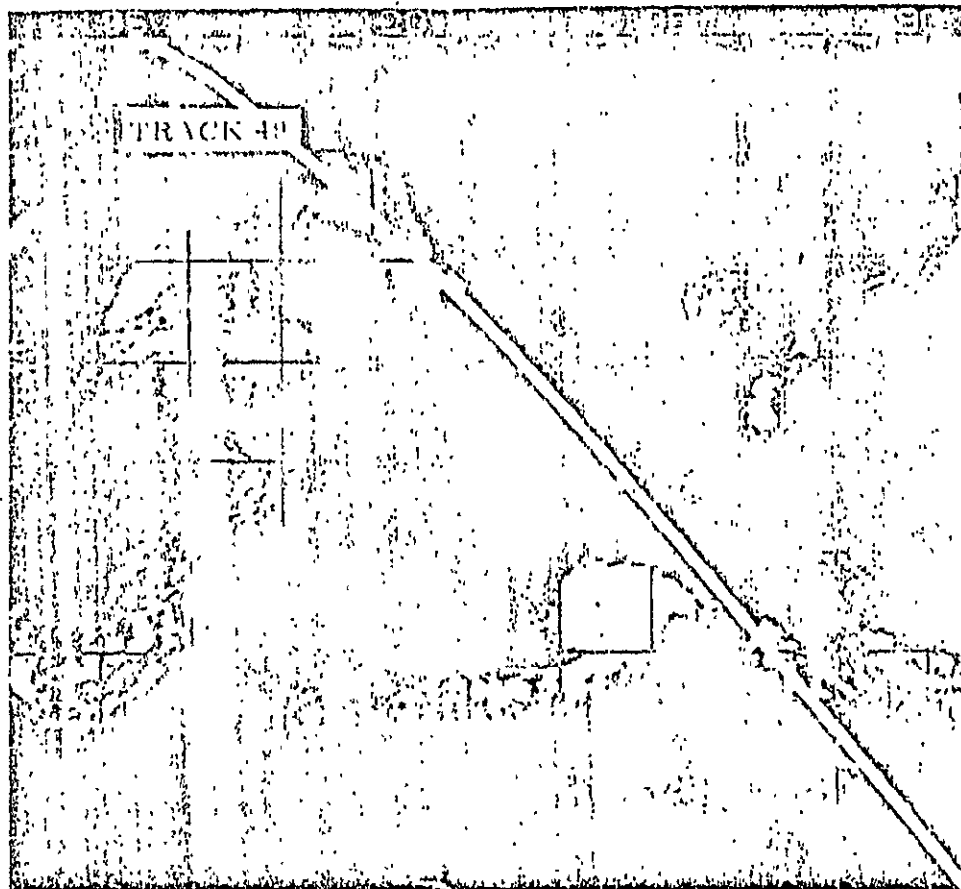


FIGURE 9. COMPOSITE VIEW OF PACIFIC HURRICANE AVA  
PROXIMITY OF THE SKYLAB SUBORBITAL TRACK.

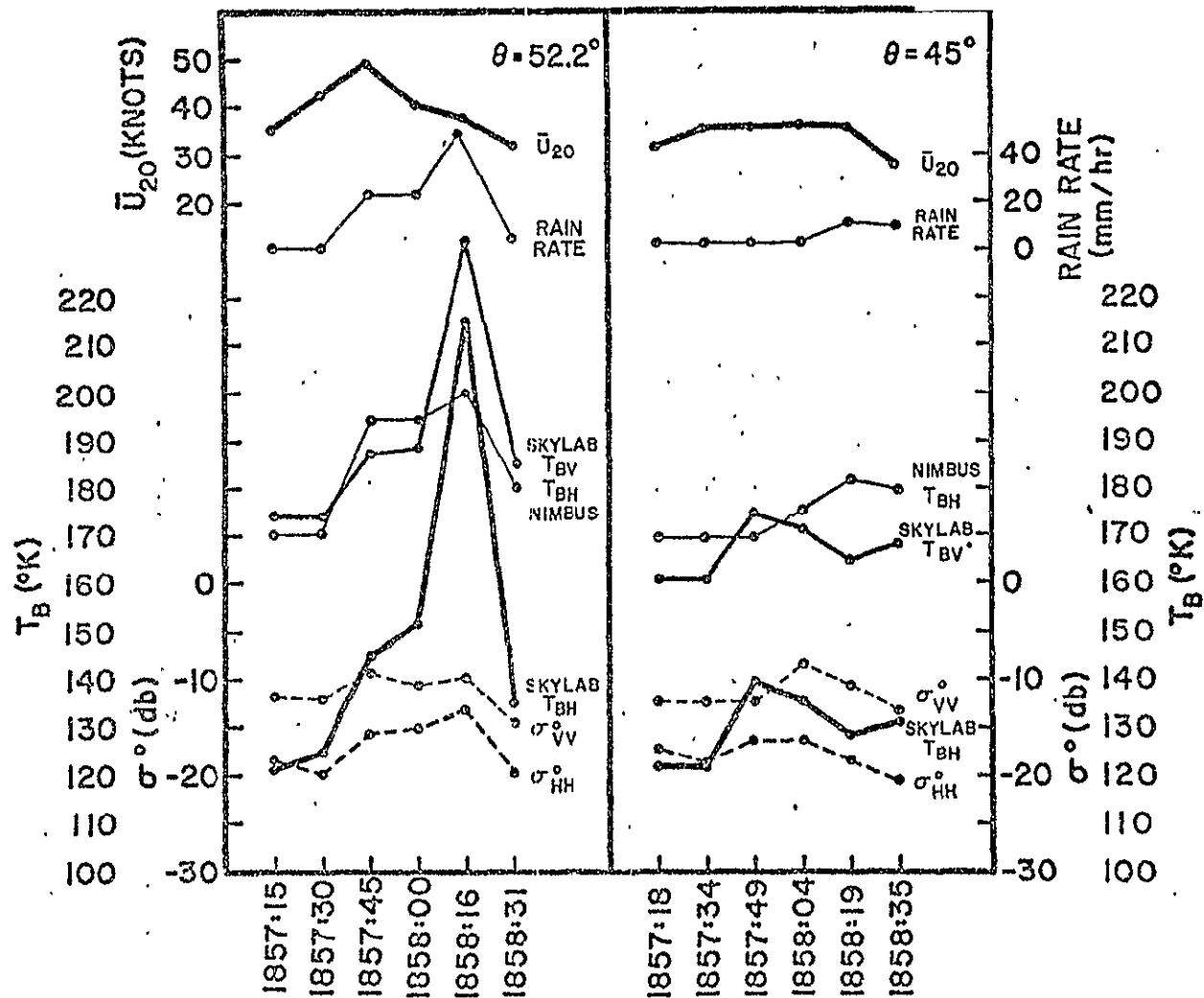


FIGURE 10. ACTIVE AND PASSIVE MICROWAVE OBSERVATIONS OF WIND FIELD IN HURRICANE AVA.

A COMPARISON OF SKYLAB S-193 AND AIRCRAFT VIEWS OF SURFACE ROUGHNESS M-2  
AND A LOOK TOWARD SEASAT

By Duncan Ross, Sea-Air Interaction Laboratory, National Oceanic and Atmospheric Administration, Atlantic Oceanographic and Meteorological Laboratories, Miami, Florida

ABSTRACT

An extensive aircraft underflight program was conducted along the Skylab ground-path for the purpose of documenting wind, wave, and atmospheric conditions affecting the amplitude of the active and passive microwave signatures. The S-193 microwave system senses a roughness parameter at the ocean surface that is proportional to the surface windspeed. The exact relationship between the wind and this roughness parameter is the subject of continuing investigations.

In the case of the active portion of the system, the intensity of off-nadir backscatter from the ocean is thought to be primarily determined by the amplitude of short gravity/capillary waves and has been shown to be strongly a function of azimuth relative to the surface wind direction. The passive side of the instrument senses the naturally emitted (and reflected) microwave energy and is proportional to the RMS slope and percent foam coverage of the ocean.

NOAA, NASA, and USAF aircraft were equipped with a variety of environmental sensors in an attempt to specify the surface conditions affecting the satellite sensors as well as active and passive microwave sensors intended to calibrate the Skylab instrument. The aircraft program is described, and some comparisons of satellite and aircraft results are presented. The principal result of the comparison of active radar is that direct inferences of the surface windspeed are possible, but subject to considerable scatter, and that this scatter appears to be due to interaction between long gravity and short Bragg waves and backscatter due to rain as well as errors in correcting for azimuth dependence. It is shown that  $\sigma_0$  for incidence angles of  $\approx 50^\circ$  increases both with windspeed and with increasing energy level of the high-frequency gravity waves that, themselves, are proportional to both the local wind and fetch in a manner that is not uniquely determined by the windspeed.

An unforeseen opportunity to observe a Pacific hurricane by both Skylab and NOAA aircraft has contributed to the development of a simplified wave forecasting scheme applicable to hurricanes, and more general conditions, which combines the better qualities of both spectral and height/period forecasting techniques. The implication of this result to the SEASAT program is that quite large data inputs in both the time and space domain can be handled using existing computers and should produce a forecast of comparable or superior quality to existing spectral techniques, but in shorter time steps. Horizontal polarization data obtained by the aircraft in Hurricane Ava, and in other experiments, which led to this development are presented.

ORIGINAL PAGE IS  
OF POOR QUALITY

### INTRODUCTION

The S-193 experiment aboard Skylab was intended to test the concept of remote determination of surface wind conditions on a worldwide basis as an aid to improved environmental forecasts. A part of this experiment included an aircraft underflight program to calibrate and validate the inference of surface wind conditions from the satellite measurements of radar backscatter,  $\sigma_0$ , and upwelling naturally emitted microwave energy,  $T_a$ .

A number of significant developments have evolved as a result of this combination of satellite and aircraft studies of the environment, which will be touched upon herein. It is impossible, however, to discuss in depth all aspects included in the scope of this program. Results presented here are preliminary, and some conclusions may be modified as additional data sets are considered. The reader is, therefore, asked to be tolerant of missing details and tentative conclusions that, hopefully, will be firmed up in future reports.

### AIRCRAFT INSTRUMENTATION

The aircraft measurements were obtained from instrumented NOAA, NASA, and USAF C130 aircraft. All aircraft were equipped with a basic environmental package consisting of an inertial platform for windspeed determination, a Barnes Infrared Radiometer for sea surface temperatures, a laser wave profiler for wave measurements, a Cambridge Dew Point Hygrometer, a Rosemount Air Temperature Probe, and a vertical camera for white-cap photography. The NOAA C130 was additionally equipped with a three-frequency passive microwave system at  $K_u$  (14.5 GHz), X (8.35 GHz), and L (1.8 GHz) bands. This system was used for dual polarization measurements at X and  $K_u$  bands and horizontal polarization measurements at L-band. Because the NOAA aircraft was not available for the third launch period, a cooperative arrangement with the Air Force 53rd Weather Reconnaissance Squadron of the Air Weather Service was negotiated by NOAA, and the inertial platform, laser, microwave, and camera systems were transferred to the Air Force C130 for the SL-4 underflight program. Figure 1 shows the NOAA C130 aircraft with passive microwave antennas extended to the in-flight operating position.

The NASA JSC C130 aircraft was similarly equipped except that the microwave system was both active and passive (time-shared) and centered only at 13.5 GHz. The NASA aircraft participated in the underflight program during all three launch periods.

### SATELLITE INSTRUMENTATION

Skylab S-193 Instrument. The S-193 experiment aboard Skylab consists of an instrument capable of operation in one of three modes: (1) short pulse altimetry, (2) radar backscatter, and (3) a passive radiometer mode. The instrument is a single-frequency device centered at 13 GHz ( $K_u$  band). In the so-called RADSCAT configuration, the instrument alternately switches between the active and passive mode. It is capable of scanning in the along-track and across-track directions, and thus obtains dual polarization measurements of radar backscattering cross section,  $\sigma_0$ , and

ORIGINAL PAGE IS  
OF POOR QUALITY

upwelling naturally emitted microwave energy, which is directly proportional to the apparent, or antenna, temperature  $T_a$ , as a function of incidence angle.

Radar Backscatter. The mechanisms responsible for determining the level of radar energy backscattered by the ocean surface are primarily, but not limited to, the amplitude of resonant Bragg waves for incidence angles between about 30° and 90°, and the RMS slope distribution for near vertical incidence angles (Wright, 1968; Valenzuela, 1968). The Bragg condition is defined as

$$\frac{2\pi}{\lambda_{\text{water}}} = K_B = K_0 \cos \theta_1 + K_0 \cos \theta_2$$

where  $\theta_1$  and  $\theta_2$  are the incident and scattering angles,  $K_0 = 2\pi/\lambda$  microwave. In the case of S-193, these waves correspond to cm wavelength ocean waves. The detailed behavior of Bragg waves and also their effect on backscatter has been the subject of considerable study in laboratory experiments in recent years (cf. Rouse and Moore, 1972; Duncan, Keller, and Wright, 1974; Keller, Larson, and Wright, 1974; Keller and Wright, 1975; Reece and Shemdin, 1974; and many others). The principal result of these studies is that the backscattered doppler radar spectrum for a particular radar frequency and incidence angle is not a unique function of windspeed but rather is, to some degree, a function of fetch, duration, and presence of swell as well as windspeed.

The Wave Spectrum. It has been suggested that the S-193 RADSCAT data are affected by both long and short ocean waves. In the following sections, an attempt will be made to evaluate S-193 data in terms of the wave spectrum. A brief description of the spectrum and its behavior during growth and swell situations is therefore appropriate.

Wave conditions can be fully described by the two-dimensional energy spectrum,  $A^2(f,\theta)$ , and integration over direction ( $\theta$ ) and frequency,  $f$ , yields the total energy

$$E = \int_0^{\infty} \int_{-\pi}^{\pi} [A(f,\theta)]^2 d\theta df$$

which is proportional to mean surface displacement,  $2\sigma^2$ .

For a wind blowing off a shoreline, the fetch is defined simply as the distance from shore to the downwind measurement site. Figure 2 presents the behavior of the one-dimensional energy spectrum for seven fetch locations during offshore wind conditions as observed in the JONSWAP experiment (Hasselmann et. al., 1973). The inset of Figure 2 depicts the meaning of the five parameters suggested by Hasselmann et. al. as convenient for describing the important characteristics of the spectrum. It can be seen from this figure that the peak frequency,  $f_m$ , grows and migrates toward lower frequencies as fetch increases. Hasselmann et. al. found that the sharpness parameter,  $\gamma$ , and the width parameters  $\sigma_a$ ,  $\sigma_b$ , are essentially independent of fetch. The Phillips parameter,  $\alpha$ , however, generally decreased with increasing fetch. The behavior of the spectral scale parameters can also be represented

4

conveniently in nondimensional form by incorporation of the local windspeed,  $U_{10}$ , and gravity. Thus, Figure 3 presents the behavior of nondimensional energy

$$\bar{E} = \frac{Eg^2}{U_{10}^4}$$

and nondimensional frequency

$$\bar{f}_m = \frac{f_m U_{10}}{g}$$

versus nondimensional fetch

$$\bar{X} = \frac{Xg}{U_{10}^2}$$

Nondimensionalization in this manner has properly accounted for the windspeed dependence of the behavior of total energy and peak frequency with fetch. The interrelationship between  $\alpha$ ,  $\bar{E}$ , and  $\bar{f}_m$  is therefore apparent and was studied in detail by Hasselmann et. al. (1975). They proposed  $\bar{f}_m$  as a convenient means of describing the stage of development of the wave spectrum in an average sense. Figures 4 and 5 from this study show the behavior of  $\bar{E}$  and  $\alpha$  with respect to  $\bar{f}_m$  and  $\bar{X}$ . The lines denoted

$$C_\omega = 10^{-3}$$

and

$$C_\omega = 10^{-5}$$

are representative of the momentum entering the wave field (Hasselmann et. al., 1973), with an approximate mean value of

$$C_\omega \approx 10^{-4},$$

or about 20 percent of the total momentum transferred to the ocean by the wind. Variations about the mean are attributed to changes in the local wind conditions. An example of varying the wind by a factor of 1.5 for a particular  $f_m$  is included in the figures.

## RESULTS

Because the principal purpose of the S-193 experiment was to remotely infer surface wind conditions, it is appropriate to first consider examples of the data from a typical pass as a prelude to more extensive analysis of the complete data set. Figure 6 presents the results of a pass in the Gulf of Mexico during SL-2 and is a typical example of variable low windspeed conditions. The S-193 active radar backscattering cross sections,  $(\sigma_0)$ , and passive microwave antenna temperature,  $T_a$ , for horizontal polarization and an incidence angle of  $50^\circ$  are shown plotted as a function of latitude along with the surface wind conditions as determined from the NOAA aircraft underflight.

Considerable variability can be seen for  $\sigma_0$ , especially around 19° and 22° N. The data for those latitudes less than 23°, however, were not corrected for azimuth dependence and therefore show scatter due to changes in wind direction as well as speed. The higher latitudes, however, are of most interest because they were accompanied by extensive ground truth. It can be seen that the surface winds decreased significantly between 24° and 26° N, while  $\sigma_0$  decreased only slightly between 24° and 25.5° N and actually increased at 26° N. The horizontally polarized antenna temperature agrees well with aircraft determinations and also increases significantly at 26° N. Because of the presence of many rain showers observed by the aircraft to be in the area of 26° N, these increases are tentatively attributed to this factor. This pass, therefore, implies significant corrections would normally be required to account for the presence of rain.

During SL-2, a unique opportunity to observe high wind conditions developed with the appearance of a hurricane in the eastern Pacific southwest of Acapulco, Mexico (Ross et. al., 1974). As plans were being formulated for observing the storm with the S-193 system, the NOAA C130 aircraft deployed on the 6th of June to Acapulco, refueled, and flew a 7.5-hour mission into the storm. Figure 7 is a NOAA-2 composite satellite view of Hurricane Ava showing the flight track of Skylab as it conducted a data pass with S-193 operating in the side-looking solar inertial mode. Unfortunately, the storm was rapidly moving away from the subsatellite track and it was not possible to obtain measurements in the region of maximum winds. Figure 8 is an example of active and passive measurements of Ava obtained at incidence angles of 42.5° and 50.5° along with estimates of surface winds obtained during the aircraft penetration and rainfall rates estimated from the NIMBUS-5 satellite 19.35 passive microwave system (Wilheit, 1972). It can be seen from this figure that there is an increase in  $\sigma_0$  and  $T_a$  in the higher wind areas of the storm with the highest antenna temperature occurring in the zone of heavy rainfall.

High wind conditions were also obtained during the third launch period. Figure 9 shows the subsatellite track for data obtained on the 9th of January at incidence angles of 0° and  $\pm 50^\circ$  along with the NOAA surface analysis for 1800Z. This situation is particularly interesting because the windspeed varied from 7.5 to 30 m/sec from the beginning to the end of the sampling period with little rainfall reported except in the region of the front. Figure 10 presents the variation in  $\sigma_0$  and  $T_a$  for +47.6° and -50.5° incidence angle along with surface winds estimated from an isotach analysis based mainly on ship reports and the NASA JSC aircraft measurements. A qualitative comparison of these data sets, together with that from Hurricane Ava and the June 11 pass in the Gulf of Mexico, strongly suggests a first-order dependency on surface wind conditions but with scatter.

Unfortunately, due to damage to the S-193 antenna occurring during an SL-3 extravehicular excursion, the antenna pattern was altered in an unknown fashion. It is therefore risky to include the 9 January data set with those obtained during SL-2 when calculating windspeed dependency. This case was therefore treated separately and is shown plotted against windspeed in Figure 11.  $\sigma_0$  and  $T_a$  data obtained during SL-2 are shown in Figure 12 plotted against windspeed. These data sets are restricted to those data passes described above, which were accompanied by an aircraft underflight. Aircraft-determined antenna temperatures included show good agreement with S-193. The surface winds attached to each satellite data point are judged to be accurate to about 1 to 3 m/sec in the case of SL-2 and 3 to 5 m/sec in the case of the SL-4 pass of 9 January. The judgment of accuracy includes the effects of mesoscale variability in the local wind conditions and inaccuracies associated with aircraft-determined winds and ship reports in the case of

**ORIGINAL PAGE IS  
OF POOR QUALITY**

the 9 January data. Unfortunately, no study is known to the author that compares ship reports (mostly visual estimates) to continuously recorded and calibrated winds averaged over 10 to 30 minutes. Therefore, one is left with a judgment.

### DISCUSSION

The above data sets strongly suggest a useful first-order relationship between surface winds for both  $\sigma_0$  and  $T_a$  subject to some degree of scatter. There are several sources of errors in both parameters contributing to the scatter that crops up in the processing. In addition, there may be errors due to invalid atmospheric assumptions (or errors in the corrections required for a particular assumption), random errors in inferring the 10-meter windspeed from aircraft measurements, as well as natural variability in local wind conditions. The above errors inherent to this data set probably cannot be reduced any further.

One potential source of error that can be addressed, however, lies in the lack of uniqueness of the active or passive signature due to the variability in possible wave conditions that may be present for a given windspeed. Reece and Shemdin (1974), in a study conducted in a wave tank, showed that the high-frequency waves, for a particular fetch, are windspeed dependent, but the absolute energy level for a particular windspeed is reduced with the addition of a low-frequency component (swell) and that the amount of the reduction is proportional to the amplitude of the low-frequency component. Mitsuyasu (1971) showed similar reduction in the high-frequency gravity region of the wave spectrum with the introduction of swell. Hasselmann et. al. (1973), showed that the Phillips constant ( $\alpha$ ) (Phillips, 1958), which determines the energy level of the  $f^{-5}$  region of the wave spectrum, decreases with increasing nondimensional fetch as discussed earlier. In order to assess the possible importance of the gravity wave spectrum in this data set, it is desirable to consider  $\sigma_0$  as a function of some observable parameter of the wave field that varies with fetch in a well-behaved and predictable manner.

The nondimensional peak frequency,  $\tilde{f}_m$ , was shown earlier to be a particularly useful parameter that well describes the stage of development of the wave spectrum. Aircraft measurements of the wave spectrum were used directly to specify  $f_m$  for Skylab data sets obtained on 5 and 11 June 1973. The data for Hurricane Ava, however, present a special problem because the aircraft measurements were not obtained at the exact subsatellite point. In order to specify the peak frequency, it was desirable to develop some technique of estimating these parameters from the aircraft data set. The hurricane wind fields are circular in nature, however, and the fetch relationship needed to infer  $\tilde{f}_m$  is ambiguous and arbitrary. Furthermore, the position of the aircraft measurements relative to the eye of the hurricane were concentrated in the rear quadrant, whereas most of the satellite positions were to the right of the hurricane center. Figure 13, however, presents some of the wave data obtained, plotted along with spectra from the North Sea measured under similar wind conditions, but fetch limited, and in the North Atlantic during fully developed conditions. The resemblance between the spectra is striking. The most significant feature of the Ava-spectra, however, is the general lack of "swell," which would appear as a secondary peak in the spectrum. This is especially significant when the unidirectional assumption required in processing the aircraft data is considered. Because we assume all waves are moving in a direction parallel to the aircraft flight track, swell from some other direction is moved toward lower frequencies in the mapping process to fixed coordinates, leading to an unrealistic "broad"

ORIGINAL PAGE IS  
OF POOR QUALITY 1916

appearance to the spectrum with multiple peaks. Hurricane Ava was a superhurricane by any criteria and had a record low pressure for eastern Pacific storms of 914 millibars. Fortunately, another such storm of which wave measurements have recently become available was Hurricane Camille, one of the worst hurricanes to ever strike the coast of the United States as it went ashore near Mobile, Alabama, in August of 1969. Camille's eye dimensions, maximum winds, forward velocity, and central pressure were virtually identical to those of Hurricane Ava. Measurements of wave conditions in relatively deep water were obtained by a consortium of oil companies. Some of the data were reported recently (Patterson, 1974, and Hamilton and Ward, 1974) and were used in this study. Figure 14 presents the relative positions of Camille and Ava wave data to the eye and wind field of Ava as determined from the NOAA aircraft flight. It is fortunate that Camille was so similar to Ava as the windspeeds measured on the oil company platform were biased low because of poor anemometer exposure for a storm approaching in the direction of Camille. Ava's winds were therefore used to specify the Camille wind field, which avoids the difficulty of introducing another empirically based technique to specify 10-meter anemometer winds. The wave data from Camille and Ava were then nondimensionalized and plotted against the nondimensional radial distance from the eye and are presented in Figure 15. It can be seen that a simple power law reasonably well describes the radial behavior of both  $\bar{E}$  and  $\bar{f}_m$ . Nondimensional peak frequencies for the Ava data set were therefore calculated from the expression.

$$\bar{f}_m = 1.6\bar{R}^{-.25}$$

where

$$\bar{R} = \frac{rg}{U_{10}^2}$$

and  $r$  is the particular radial distance from the subsatellite point to the eye of Ava. The Ava data set was then combined with data from 5 and 11 June 1973 and is shown in Figure 16. It can be seen that  $\sigma_0$  varies considerably with  $\bar{f}_m$ . It can be argued that, because the windspeed is included in the calculation of  $\bar{f}_m$ , it is difficult to correctly separate the windspeed dependency from stage of development. To aid in this separation of dependencies, a multiple regression analysis was performed according to the equation

$$Z = a_0 + a_1x + a_2y$$

letting  $Z = \sigma_0$ ,  $x = U_{10}$ , and  $y = \bar{f}_m$ . The constants  $a_0$ ,  $a_1$ , and  $a_2$  were found to be -29.5, 0.20, and 59.4, respectively. Such a dependency on  $\bar{f}_m$  is much greater than expected or would be predicted on the basis of wave tank experiments cited earlier. The same multiple regression analysis was performed on the 9 January data set, based on hindcast  $\bar{f}_m$ , for 47.6° incidence angle, and yielded values of -15.7, 0.39, and 17.5 for the same constants. The hindcast performed assumed limited fetch, but unlimited duration, and the rather low wave heights reported suggest an underestimate for the values of  $\bar{f}_m$  for the higher winds. Also possible is a bias in the case of the hurricane data set due to backscatter from rain. The 9 January data set, however, seems to confirm a fetch dependency and both sets considered together suggest that controlled high-wind, variable-fetch experiments should be performed to accurately infer high winds from measurements of  $\sigma_0$ .

ORIGINAL PAGE IS  
OF POOR QUALITY

A similar treatment of the fetch effect in the case of the passive microwave measurements is also indicated and is underway.

#### RELATION TO SEASAT

The success of the simplified approach suggested by Hasselmann et. al. (1975) for specifying the evolution of the wave spectrum depends on successful parameterization of the nonlinear interactions that control the exchange of energy within the spectrum that, in turn, are very sensitive to local gustiness in the surface wind conditions. However, because it is not necessary to deal with the entire directional spectrum for each grid point in a numerical forecast scheme, it will be possible to increase the density of grid points and decrease the time steps involved in forecasting waves. For example, a typical spectral model consisting of 17 frequencies and 15 directions for 512 grid points in the North Atlantic requires 130 000 storage locations, whereas the simplified approach, expanded to account for two swell systems, can increase the grid density to 5012 and require only 30 072 locations. Such a forecasting approach is needed for rapid assimilation of satellite data and will likely be in operation by the time the SEASAT satellite is launched. At this time, the First Global GARP Experiment will also be underway and provide a unique opportunity to test the SEASAT concept.

#### CONCLUSIONS

The Skylab S-193 experiment has proved that active and passive microwave sensors can be used to infer surface winds but are subject to scatter and a decreasing sensitivity with increasing windspeed in the case of the active radar, and bias due to rainfall with little sensitivity to lower windspeeds in the case of passive microwave signatures. These results, therefore, suggest that combined active and passive systems with a weighted averaging process (employing polarization dependencies) being used to infer the local wind might reduce some of the scatter due to random errors and should be tested with Skylab data. The results further suggest that a parameterization of the wave spectrum may be necessary in order to further reduce the scatter in  $\sigma_0$ . The Skylab data set contains most of the data needed to test these hypotheses and could lead to satellite determination of both the windspeed and surface wave spectrum by judicious use of active and multifrequency passive microwave systems.

#### ACKNOWLEDGMENTS

The author is grateful to the many people in the satellite and aircraft program which comprised the Skylab experiment. Special thanks are due the NOAA C130 crew for expertly conducting 500 foot flight tracks in one of the most severe hurricanes of record, and the NASA JSC and USAF air crews for low-level flights into severe winter storms (especially the Air Force loadmaster who finally closed a balky cargo door allowing a planned high-altitude pressurized return to shore during one occasion). Finally, the accuracy and extent of passive microwave data collected by the NOAA and USAF aircraft is due to the diligence and competence of the Naval Research Laboratory and is greatly appreciated.

REFERENCES

Barnett, T. P., and J. C. Wilkerson (1967), On the generation of ocean wind waves as inferred from airborne radar measurements of fetch-limited spectra. *J. Mar. Res.* 25, 292.

Duncan, J. R., W. C. Keller, and J. W. Wright (1974), Fetch and wind speed dependence of Doppler spectra. *Radio Science* 9, No. 10, 809-819.

Hamilton, R. C., and E. G. Ward (1974), Ocean data gathering program-quality and reduction of data. *Offshore Technology Conference Proceedings, OTC 2108-A*, 750-756.

Hasselmann, K., T. P. Barnett, E. Bouws, H. Carlson, D. E. Cartwright, K. Enke, J. A. Ewing, H. Gienapp, D. E. Hasselmann, P. Kruseman, A. Meerburg, P. Muller, D. J. Olbers, K. Richter, W. Sell, and H. Walden (1973), Measurements of wind-wave growth and swell decay during the Joint North Sea-Wave Project (JONSWAP), *Deutsche Hydrogr. Z., Suppl. A(8°)*, No. 12.

Hasselmann, K., D. B. Ross, P. Mueller, and W. Sell (1975), A Parametrical Wave Prediction Model, submitted to *Journal of Physical Oceanography*.

Keller, W. C., T. R. Larson, and J. W. Wright (1974), Mean speeds of wind waves at short fetch. *Radio Science* 9, No. 12, 1091-1100.

Keller, W. C., and J. W. Wright (1975), Microwave scattering and the straining of wind-generated waves. *Radio Science* 10, No. 2, 139-147.

Mitsuyasu, H. (1971), Observations of the wind and waves in Hakata Bay. *Rep. Res. Inst. Appl. Mech., Kyushu University*, 19:37-74.

Patterson, M. M. (1974), Oceanographic Data from Hurricane Camille. *Offshore Technology Conference Proceedings, OTC 2109*.

Phillips, O. M. (1958), The equilibrium range in the spectrum of wind generated waves. *J. Fluid Mech.* 4(4), 426-434.

Pierson, W. J., and L. Moskowitz (1964), A proposed spectral form for fully developed wind seas based on the similarity theory of S. A. Kitaigorodskii. *J. Geophys. Res.* 69, 5181-5190.

Reece, A. M., and O. H. Shemdin (1974), Modulation of capillary waves by long waves. *Symposium on Ocean Wave Measurement and Analysis, Amer. Soc. Civil Eng., New Orleans, Louisiana*.

Ross, D., B. Au, W. Brown, and J. McFadden (1974), A remote sensing study of Pacific Hurricane Ava. *Ninth International Symposium on Remote Sensing of Environment Proceedings, 15-19 April*, 163-180.

Ross, D., and V. Cardone (1974), Observations of oceanic whitecaps and their relation to remote measurements of surface wind speed. *J. Geophys. Res.* 79, No. 3, 444-452.

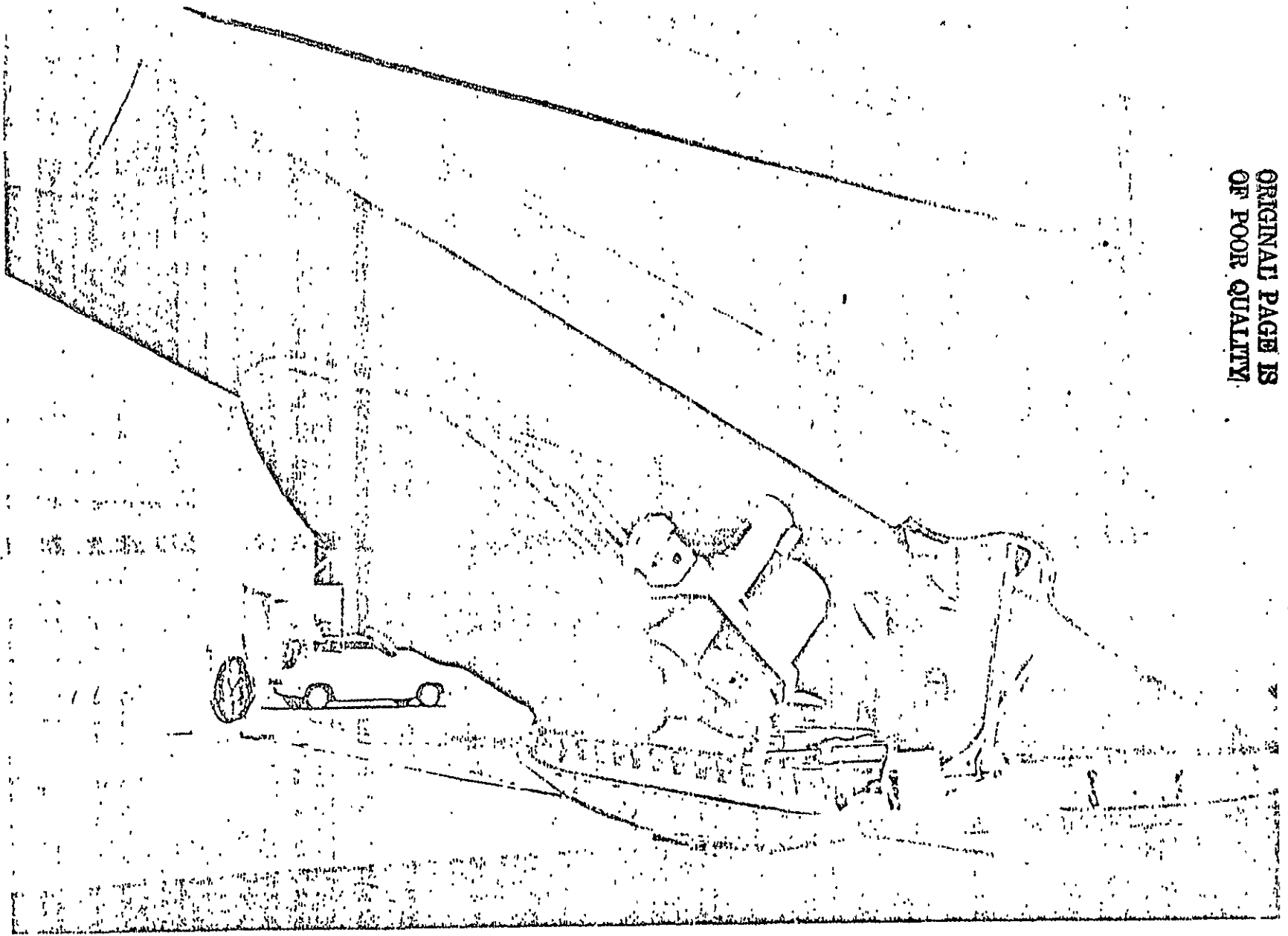
Rouse, J. W., and R. K. Moore (1972), Measured surface spectrum dependence of back-scattering from rough surface. IEEE Trans. Antennas Propagat., AP-20, 211-214.

Valenzuela, G. R. (1968), Scattering of electromagnetic waves from a tilted, slightly rough surface. Radio Science 3, 1057-1066.

Wilheit, T. (1972), Nimbus-5 Users Guide, NASA Goddard Space Flight Center, Washington, D.C.

Wright, J. W. (1968), A new model for sea clutter, IEEE Trans. Antennas Propagat., AP-16, 217-223.

ORIGINAL PAGE IS  
OF POOR QUALITY



1921

Figure 1. The NOAA C130 aircraft show passive microwave sensors in the extended position.

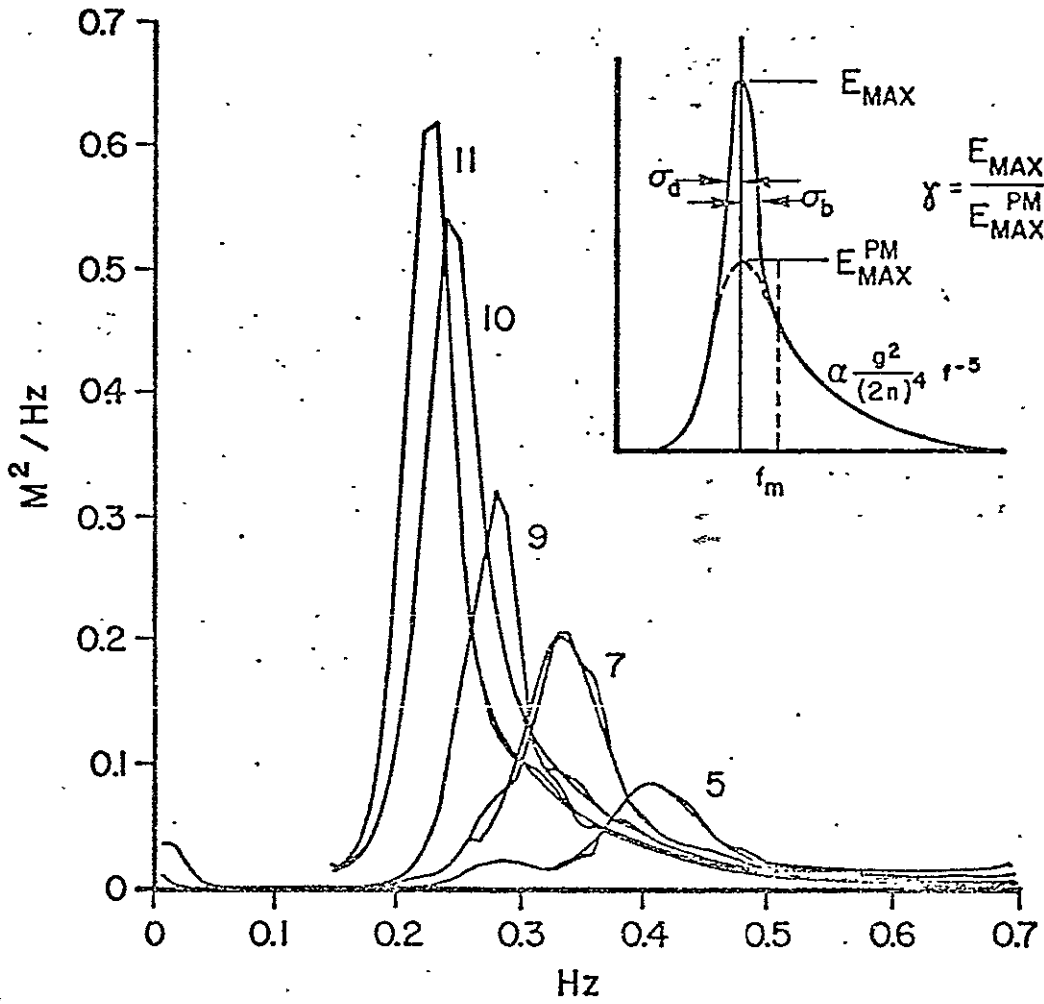


Figure 2. Growth of wave spectra for offshore wind conditions during JONSWAP-69. Fetch increases from Station 5 through Station 11. Three shape parameters  $\sigma_a$ ,  $\sigma_b$ , and  $\gamma$ , and the scale parameters  $f_m$  and  $\alpha$  suggested by Hasselmann are shown in the inset.  $\gamma$  is simply the ratio of the energy at  $f_m$  to that which would be predicted by the Pierson-Moskowitz (1964) form of the spectrum.

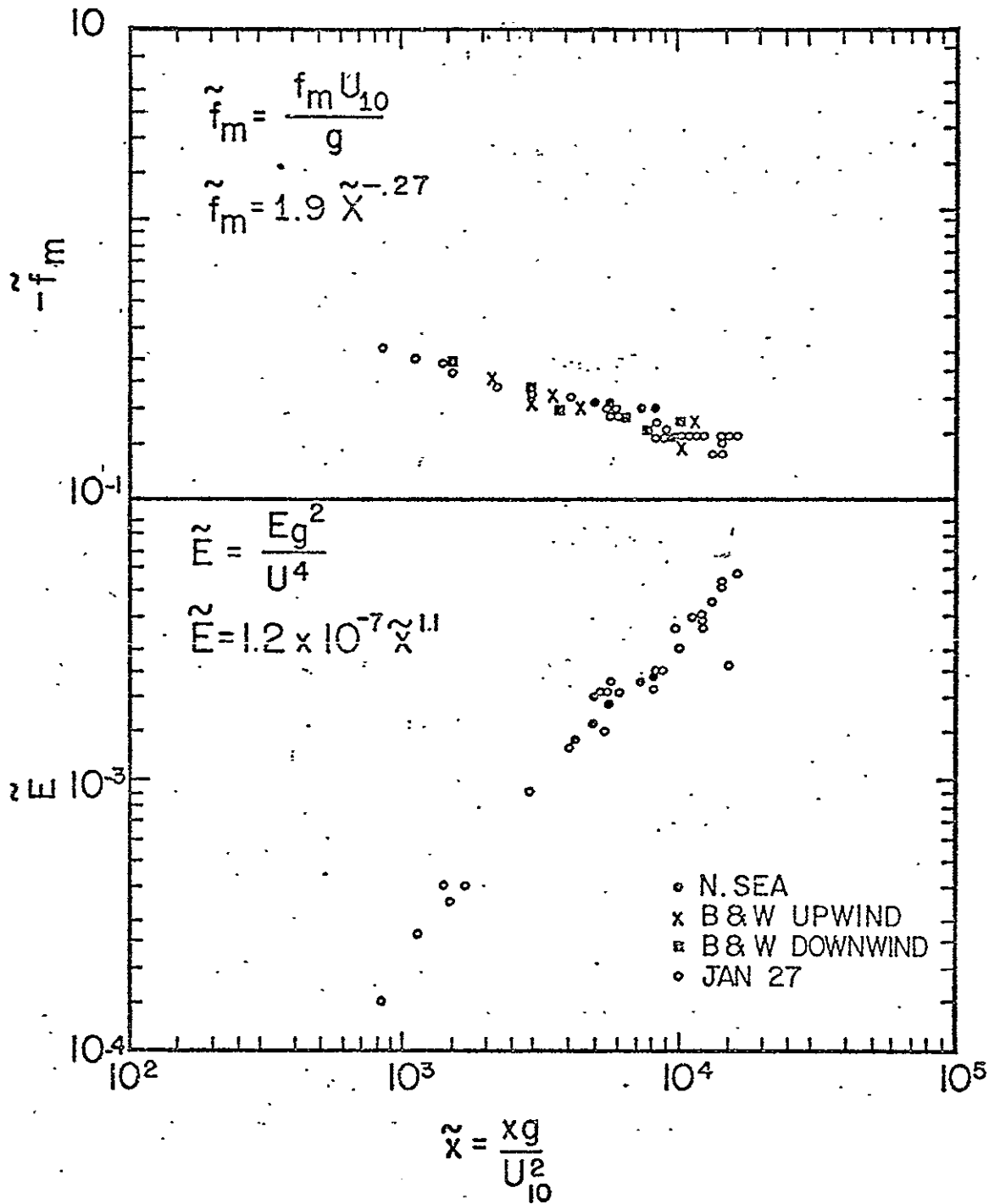


Figure 3. Dimensionless parameters  $\tilde{E}$  and  $\tilde{f}_m$  versus dimensionless fetch  $\tilde{X}$  for high wind-speeds (15 to 25 m/sec) as determined by aircraft experiments in the North Sea and off Cape Fear, N. C., on 27 January (Ross and Cardone, 1974, and Barnett and Wilkerson, 1969).

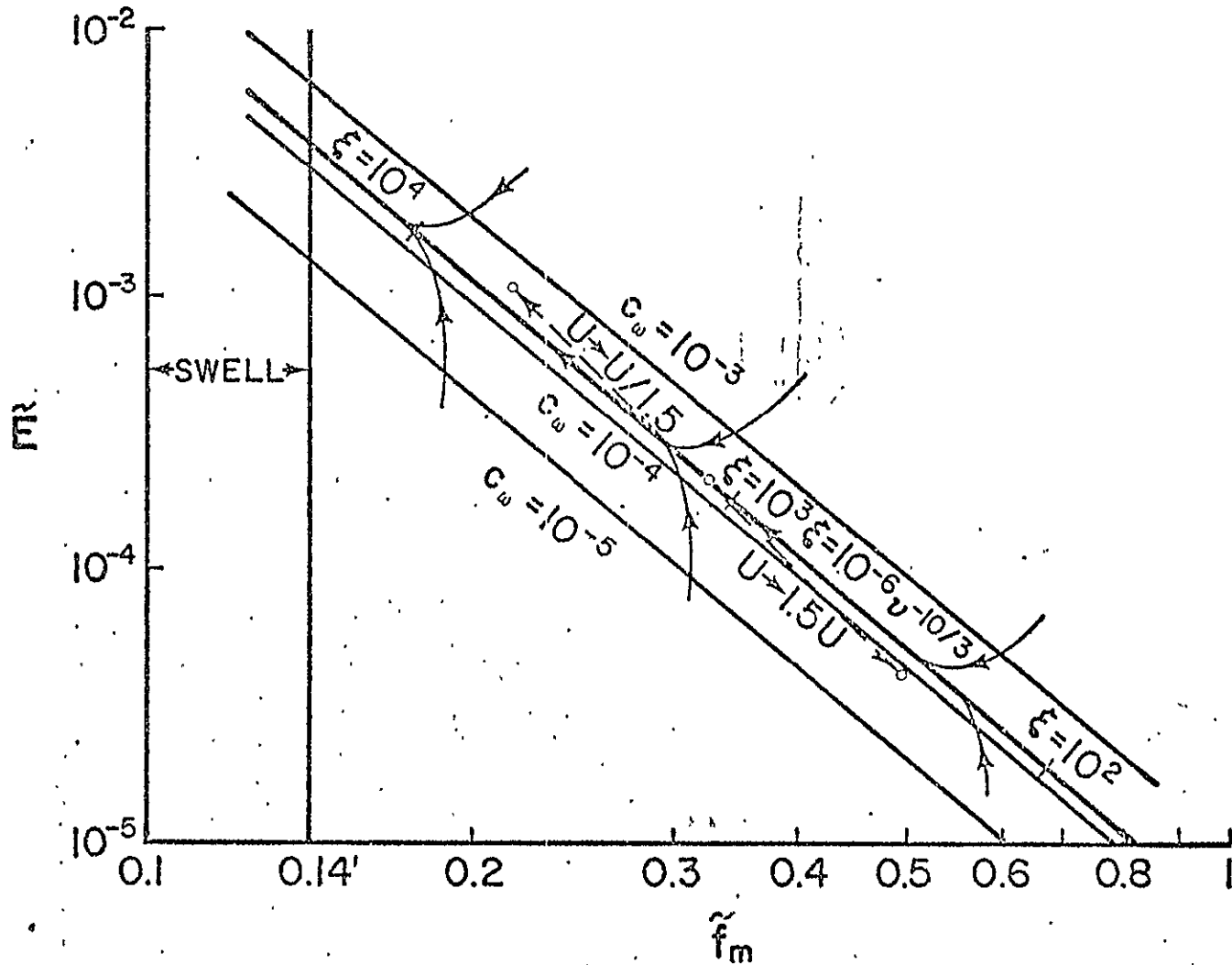


Figure 4. The behavior of  $\tilde{E}$  and  $\tilde{f}_m$  during growth. A sudden change of windspeed by a factor of 1.5 results in a departure from the mean followed by readjustment to mean condition along the curved lines indicated. Nondimensional fetch relationships  $\tilde{X} = E = \frac{\chi g}{U_{10}^2}$  for particular  $\tilde{f}_m$  are included. The upper and lower boundaries ( $C_w = 10^{-3}$  and  $C_w = 10^{-5}$ ) represent the limits of momentum being transferred to the wave spectrum.

aries ( $C_w = 10^{-3}$  and  $C_w = 10^{-5}$ ) represent the limits of momentum being transferred to the wave spectrum.

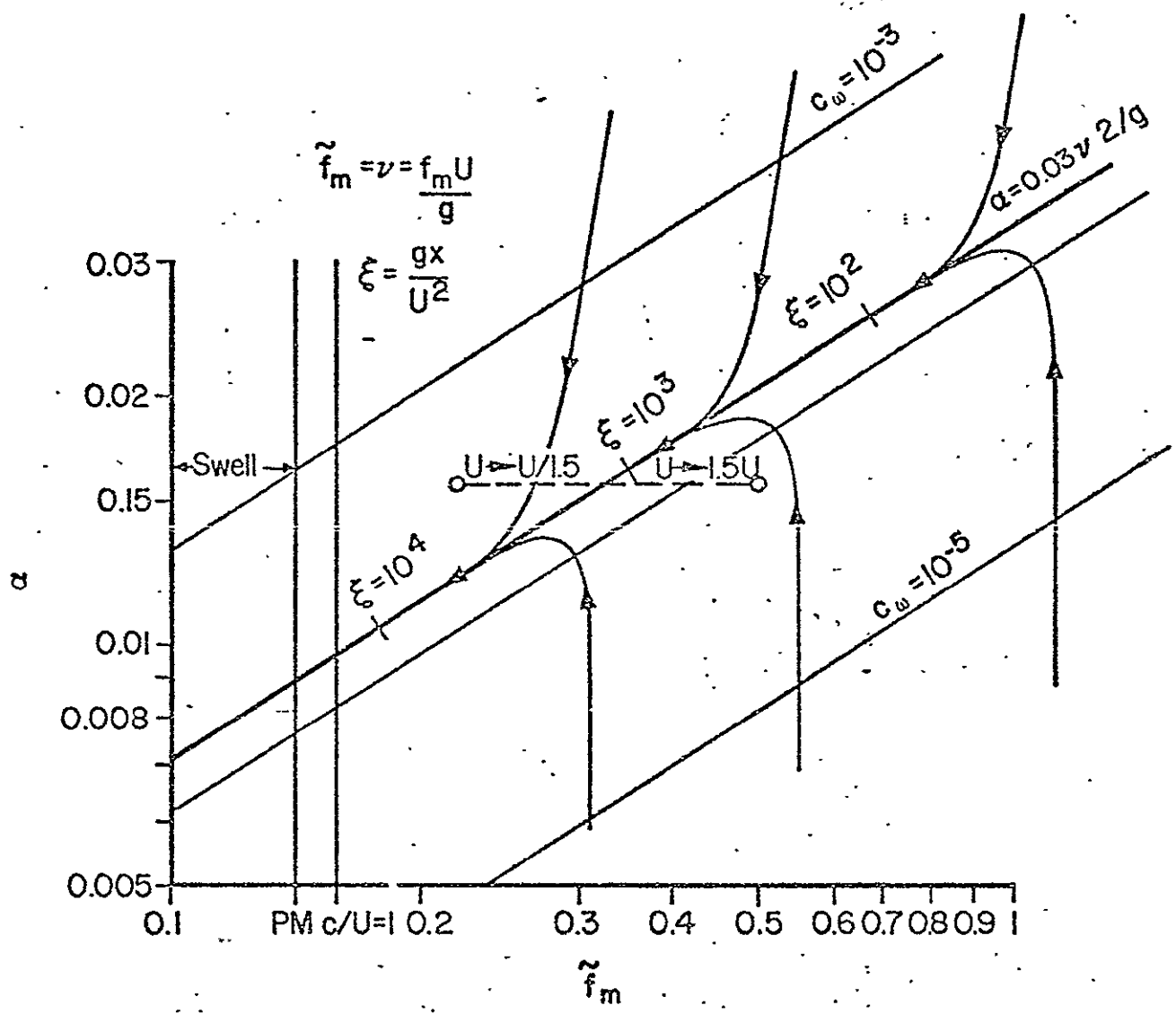


Figure 5. The Phillips parameter  $\alpha$  versus  $\tilde{f}_m$ . Corresponding fetches  $\xi$  are indicated by the tick marks. The behavior of  $\alpha$  during readjustment to a change in local wind ( $U$ ) conditions is along the curved lines.

1926

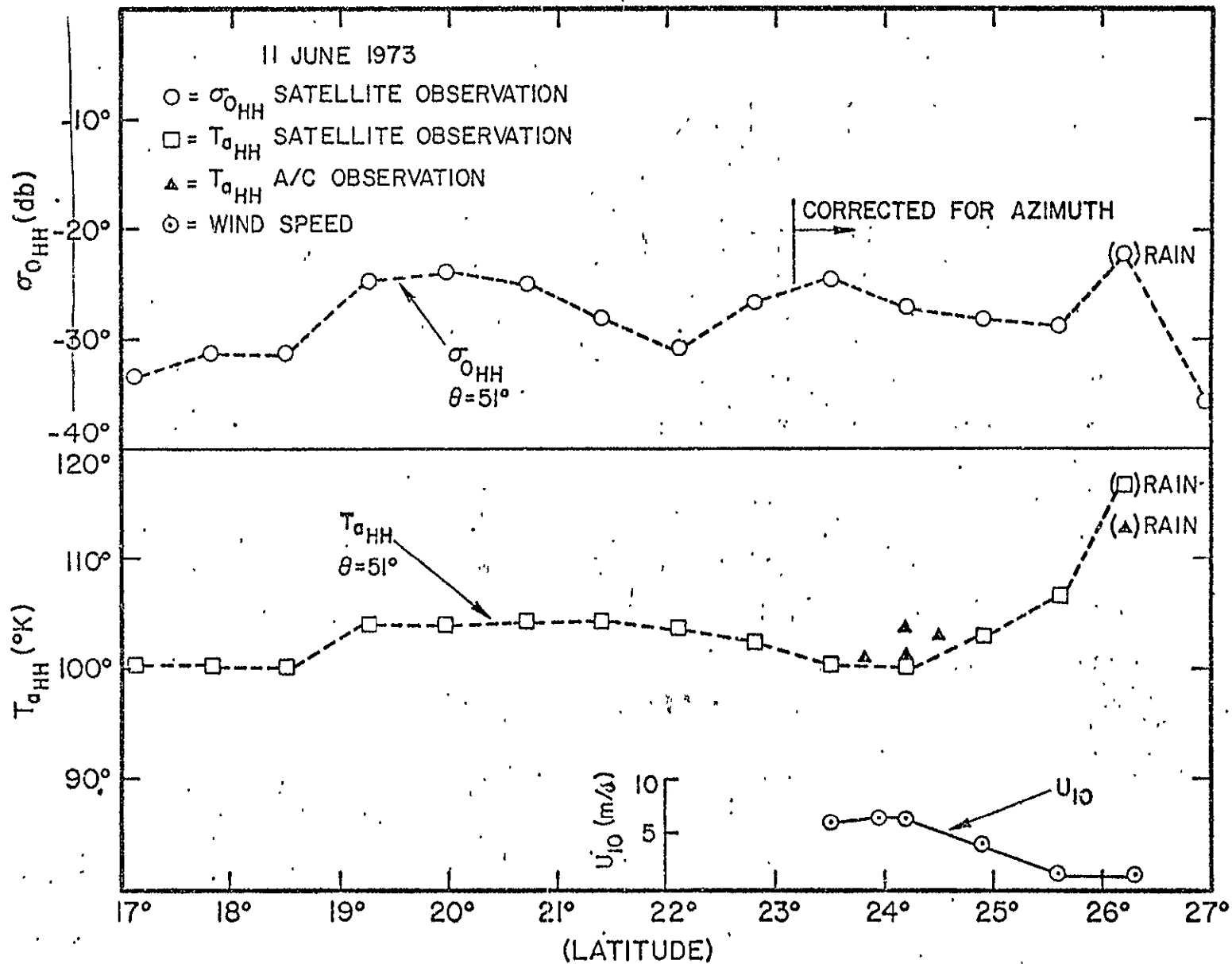
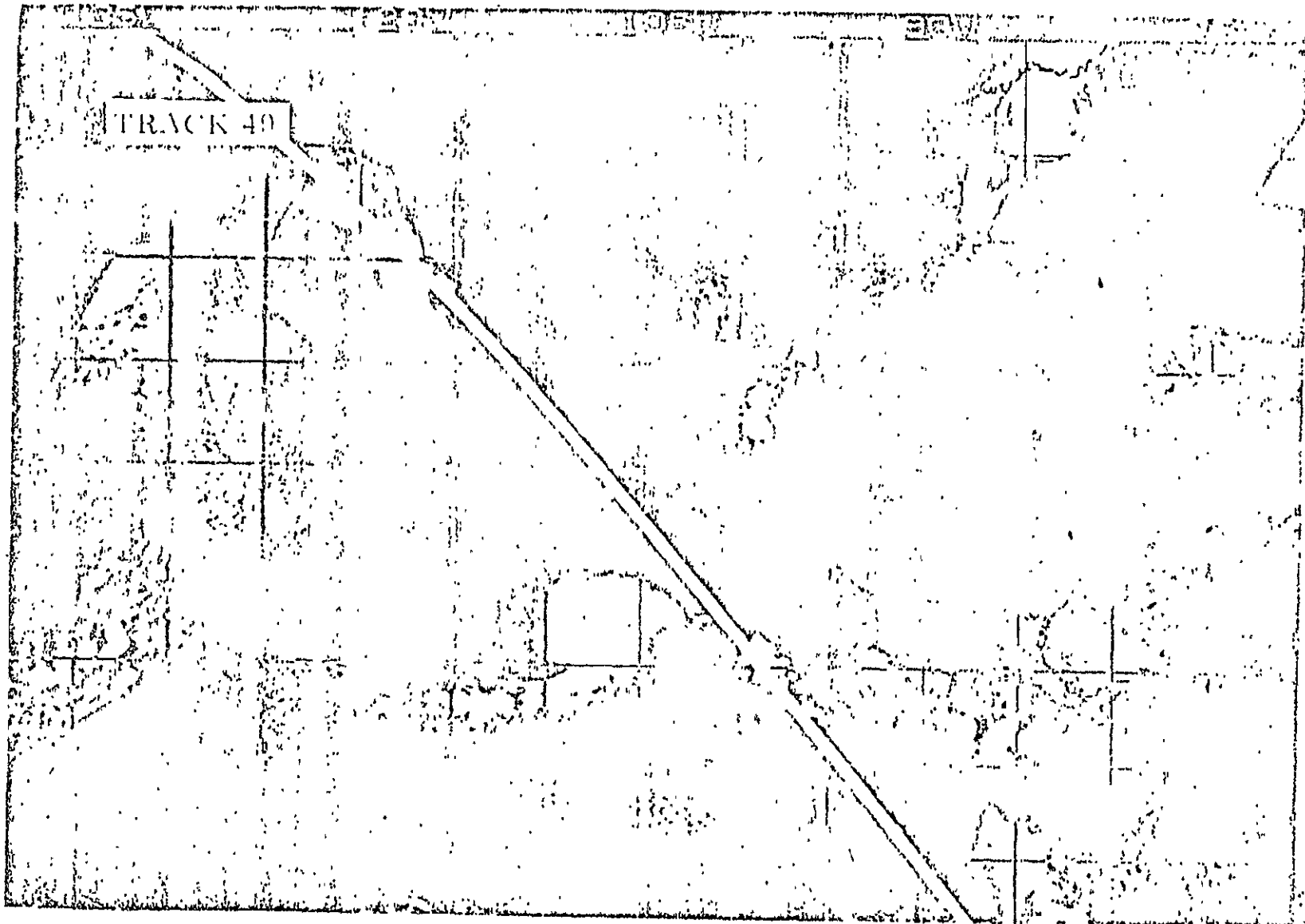


Figure 6. Skylab pass of 11 June in the Gulf of Mexico.



1927

HURRICANE AVA, JUNE 6, 1973, NOAA 2 COMPOSITE

Figure 7. Hurricane Ava, June 6, 1973, NOAA-2 composite showing track of Skylab satellite.

ORIGINAL PAGE IS  
OF POOR QUALITY

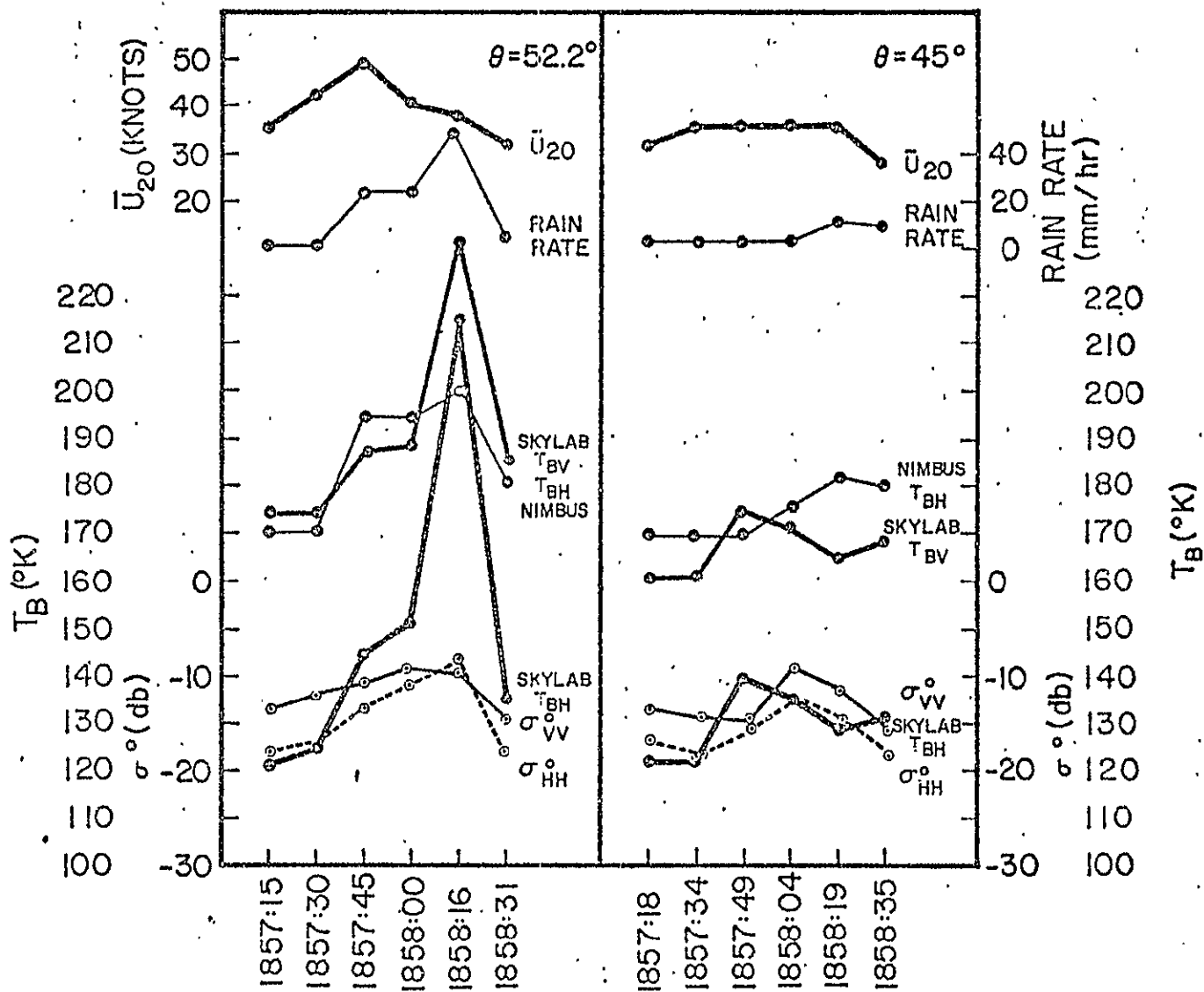
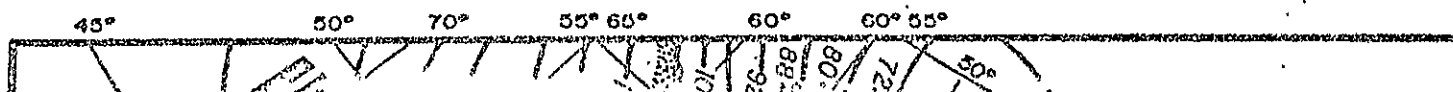


Figure 8. Skylab and NIMBUS-E data in Hurricane Ava.





1930

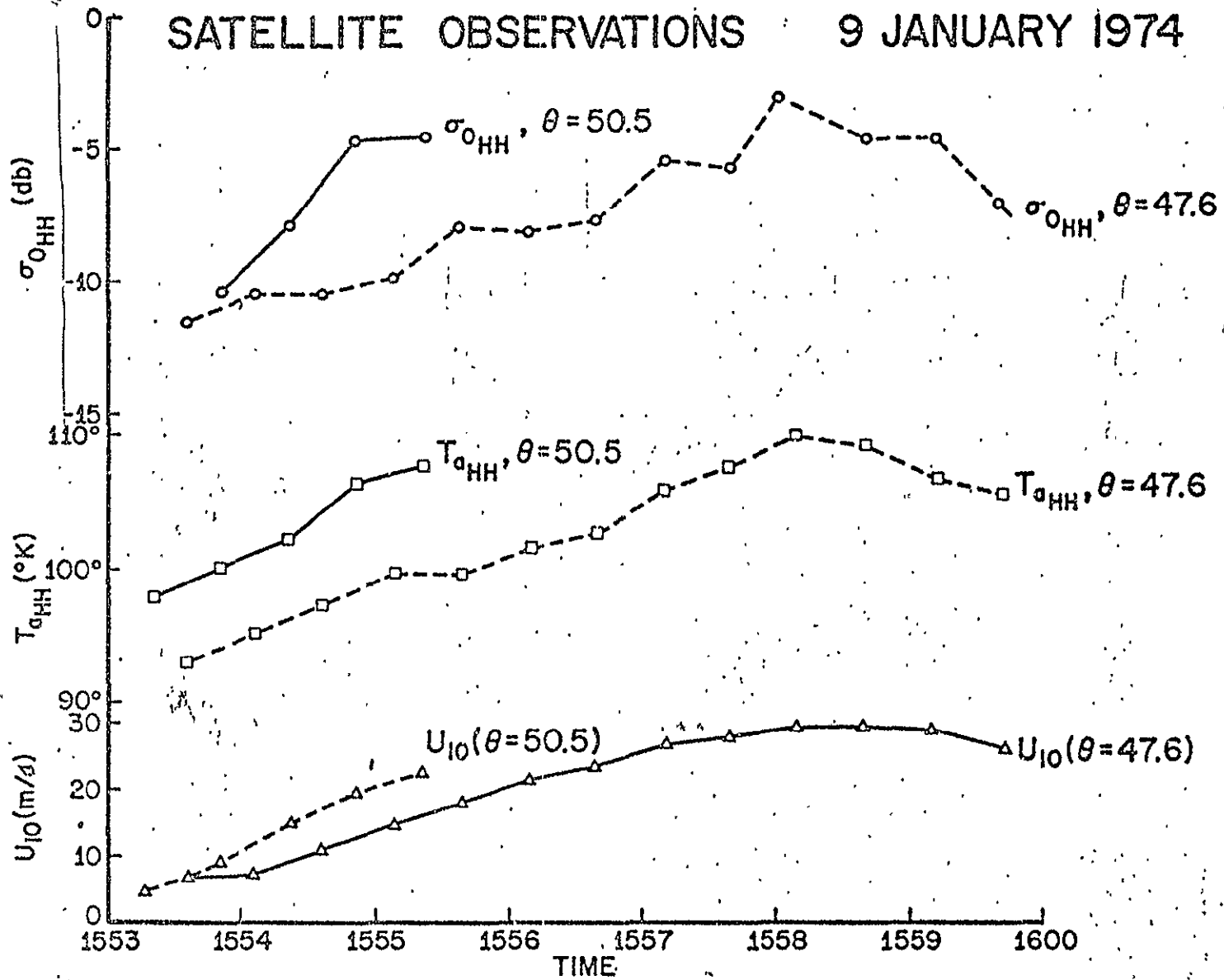


Figure 10. S-193 data during the 9 January pass along with surface winds determined from the surface analysis.

1931

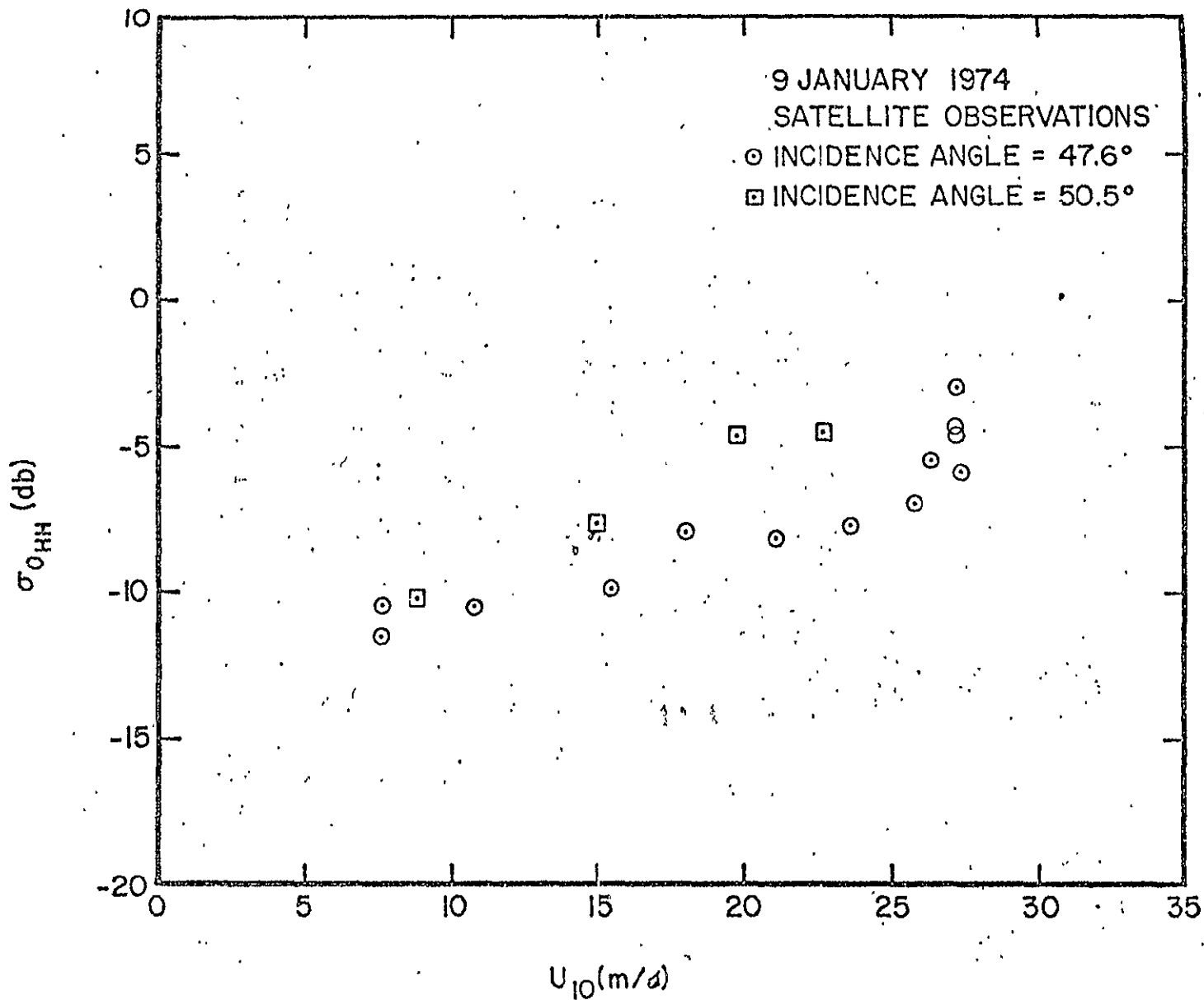


Figure 11. Radar backscatter,  $\sigma_0$  versus windspeed for 9 January.

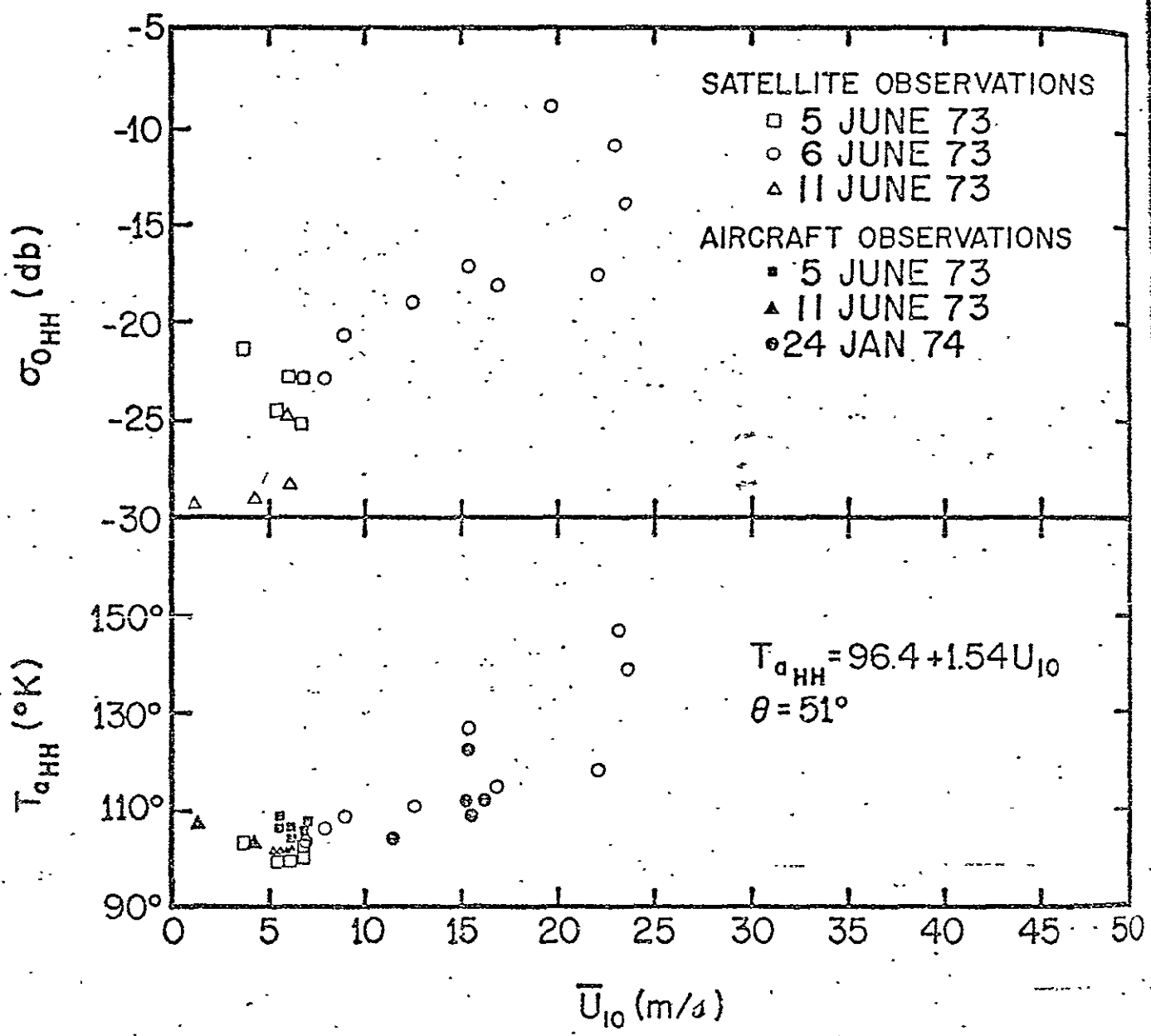
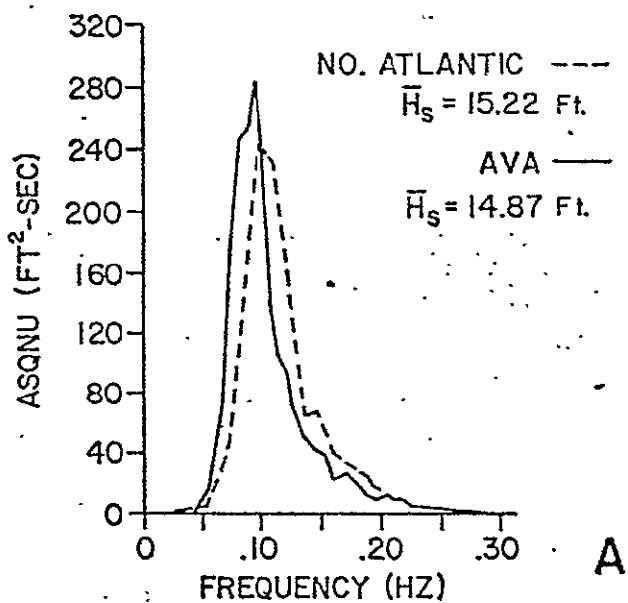
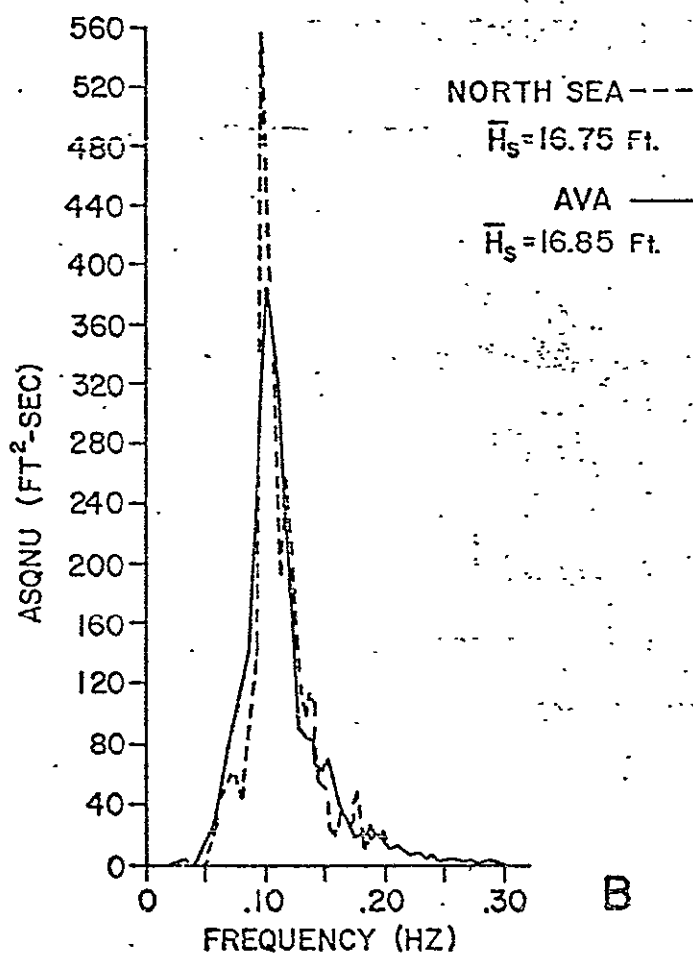


Figure 12. Radar backscatter and antenna temperature versus windspeed during SL-2.

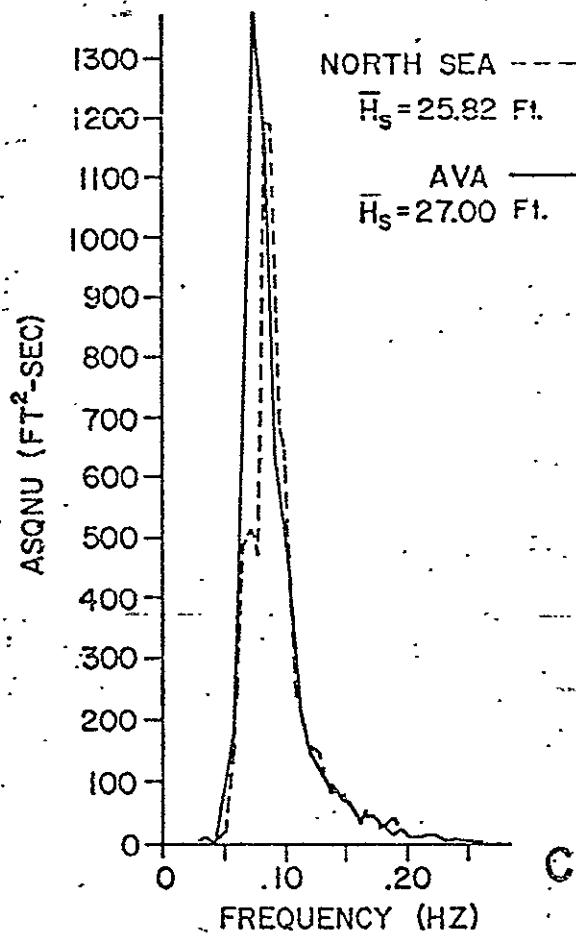
Fig



A



B



C

Figure 13. Wave spectra measured during the aircraft penetration of Hurricane Ava along with North Sea spectra for fetch-limited 25 m/sec winds.

ORIGINAL PAGE IS  
OF POOR QUALITY

1934

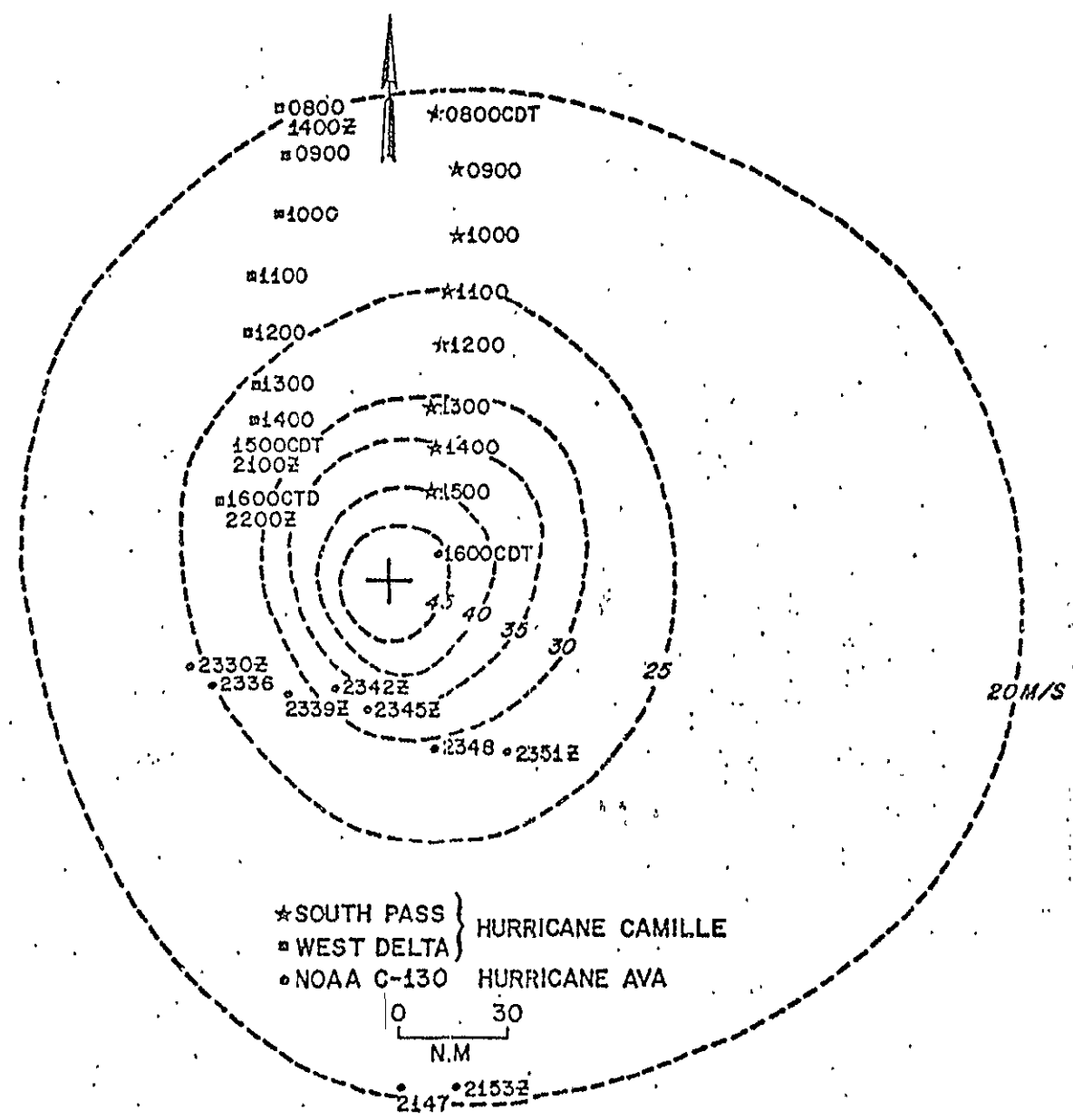


Figure 14. Surface wind analysis for hurricane Ava constructed from aircraft data along with relative positions of wave data obtained in Ava and for Hurricane Camille.

with relative positions of wave data obtained in Ava and for Hurricane Camille.

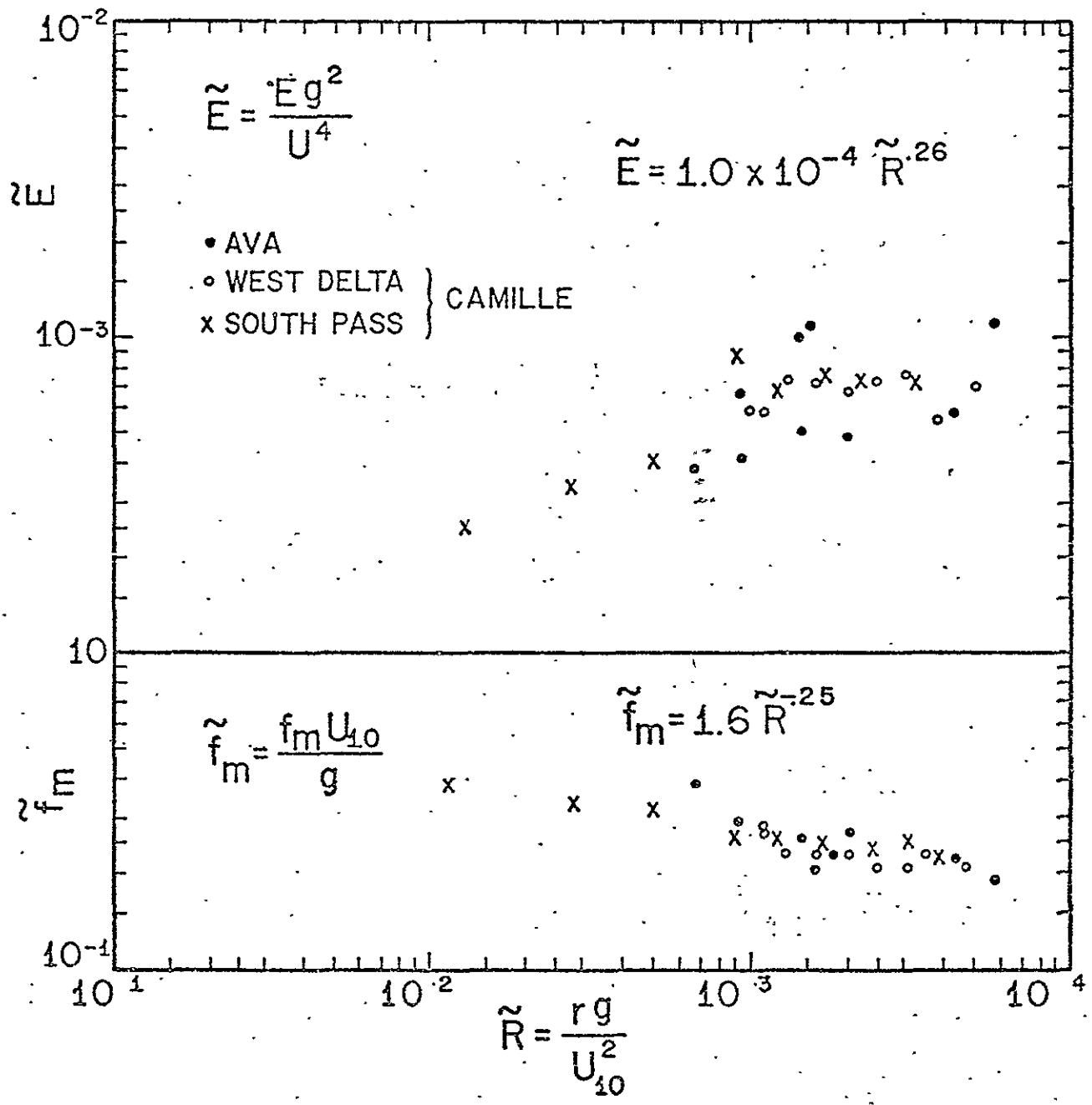


Figure 15. Behavior of nondimensional energy,  $\tilde{E}$ , and peak frequency,  $\tilde{f}_m$ , versus radial distance from eye.  $\tilde{R} \approx 10^2$  constitutes the region of maximum winds.



